Arctic Science

OPEN ACCESS | Research Article

Submergence influences higher shoreline retreat rates in complex low-lying tundra coasts (Tuktoyaktuk Peninsula, NWT, Canada)

Bernardo Costa[a], **Gonçalo Vieira**[a], **Dustin Whalen**[b], **and Michael Lim**[c]

[a]Centro de Estudos Geográficos, Laboratório Associado TERRA, Instituto de Geografia e Ordenamento do Território, Universidade de Lisboa, Lisbon, Portugal; [b]Geological Survey of Canada Atlantic, Natural Resources Canada, Dartmouth, NS, Canada; [c]Northumbria University, School of Engineering, Physics and Mathematics, Newcastle upon Tyne, United Kingdom

Corresponding author: **Bernardo Costa** (email: bcosta4@edu.ulisboa.pt)

Arctic Science Downloaded from cdnsciencepub.com by ENR-ITILIBBF on 10/30/26

Abstract

This study assesses shoreline change dynamics along a 633 km coastal stretch of the Tuktoyaktuk Peninsula, Beaufort Sea (Canada), using aerial photography-derived orthomosaics (1950 and 1985) and very high-resolution Pléiades satellite imagery (2020). We (1) characterised backshore and foreshore morphologies, (2) analysed spatiotemporal shoreline change rates, and (3) identified the morphology influence on shoreline evolution. The average shoreline change rate was −0.77 m/year (1950–2020), with a 31% increase since 1985, affecting 57% of the area. Shoreline retreat affected at least 83% of the shoreline in each sector, with the highest rates in the central sectors of the peninsula. Coastal morphology was the main factor influencing spatial variability and the dominant shoreline retreat processes. Tundra flats showed the highest retreat rates in the backshore and foreshore, with 38% land loss, despite covering 29% of the peninsula. These results challenge erosion-centric models of Arctic coastal change, highlighting coastal submergence as a dominant process in low-lying coasts. The erosion-submergence distinction is critical for improving predictive models and adaptation strategies in vulnerable communities like Tuktoyaktuk. Future research must integrate subsidence measurements, sea-level rise, inundation impacts and coastal morphology to address gaps in submergence assessment and improve shoreline change models and impacts on Arctic coastal systems.

Key words: Arctic coastal change, remote sensing, shoreline change, coastal morphology

1. Introduction

The average Arctic shoreline retreat rate of −0.5 m/year (1950–2000) has accelerated since 2000 due to climate-driven environmental changes (Lantuit et al. 2012). Key drivers include reduced sea ice extent/thickness (Barnhart et al. 2014*b*; Casas-Prat et al. 2024), larger open-water seasons (Barnhart et al. 2016; Trishchenko et al. 2022), rising sea temperatures (Timmermans and Labe 2020; Yang et al. 2023), sea level rise (Meyssignac and Cazenave 2012), and increased storminess and wave heights (Casas-Prat and Wang 2020; Kim et al. 2021) leading to large areas of periodic coastal flooding. These environmental drivers amplify shoreline retreat by triggering local controls such as ground ice thaw, permafrost subsidence, and a negative sediment budget (Irrgang et al. 2018, 2022; Berry et al. 2021), while other geomorphic factors such as nearshore slope, shoreline orientation, and cryolithology also influence shoreline change rates (Irrgang et al. 2022; Tanguy et al. 2023).

In sandy beach and foredune systems, pre-existing morphology, dune height, and alongshore variations in beach profile influence storm response and overwash patterns (Houser et al. 2008; Itzkin et al. 2021). In Arctic permafrost bluffs, erosion occurs through thermo–denudation and thermo–abrasion (Hoque and Pollard 2009; Lantuit et al. 2012; Günther et al. 2013, 2015; Irrgang et al. 2022). Thermo–denudation involves downslope movement of ice–rich soil and debris following ground-ice thaw, promoting mass wasting (Lantuit et al. 2012; Günther et al. 2013; Lim et al. 2020). Thermo–abrasion results from the combined mechanical and thermal action of waves and currents at the bluff toe, eroding and thermally degrading ice–rich sediments, thereby causing block failure and headwall retreat (Günther et al. 2013, 2015; Irrgang et al. 2022). Low-lying tundra coasts are less affected by thermo–denudation and thermo–abrasion. In these regions, shoreline retreat is driven by permafrost thaw subsidence, glacial isostatic adjustment (GIA)–related subsidence, storm surge flooding, ongoing permafrost degradation, and sea level rise (Günther et al. 2015; Lim et al. 2020; Irrgang et al. 2022; Creel et al. 2024). Storm surge events cause a dynamic shift in shoreline position, repeatedly flooding coastal lowlands and accelerating active–layer degradation, thereby driving permafrost thaw and increasing the vulnerability of low-lying terrain to future flooding (Vermaire et al. 2013; Lim et al. 2020; Kim et al. 2021; Creel et al. 2024). This repeated in-

Arctic Science Downloaded from cdnsciencepub.com by ENR-ITILIBBF on 10/30/26

teraction between short-term storm-driven flooding and permafrost degradation strengthens the link between episodic water-level changes and long-term subsidence (Günther et al. 2015; Creel et al. 2024).

The scarcity of very high-resolution (VHR) spatial data (ground sampling distance—GSD below 2 m) poses a challenge in some Arctic regions. For example, this study relies on the only VHR imagery (1950 and 1985 NAPL air photos) available for the entire Tuktoyaktuk Peninsula before the availability of VHR satellite data. VHR satellite imagery enables the detection of fine-scale coastal features and shoreline changes as small as 5 m, which medium-resolution platforms (10–60 m GSD) like Landsat (30 m GSD) and Sentinel (10 m GSD) cannot assess (Doherty et al. 2022; Vitousek et al. 2023; Vos et al. 2023). Quantitative assessments show that VHR imagery provides lower shoreline uncertainty than medium-resolution imagery, which usually have horizontal errors of up to 14 m (Smith et al. 2021; Doherty et al. 2022; Tuck et al. 2024). This accuracy is especially important in complex settings such as the low-lying tundra shoreline in the Tuktoyaktuk Peninsula (Smith et al. 2021). Previous studies on the Tuktoyaktuk Peninsula have focused on small sectors, overlooking the coastal complexity across most of the peninsula. Solomon (2005) estimated a −0.75 m/year coastal change rate for 1972–2000 in the Mackenzie Delta region, while O'Rourke (2017) studied the Kugmalit Bay and found a change rate of −0.6 m/year for 1950–2004.

Despite widespread research on Arctic coastal erosion since the 1950s, shoreline retreat has been mainly interpreted as caused by erosion, an approach with impacts for sediment (including carbon, nutrient or contaminant) flux estimation. The same occurs in modelling approaches, where changes associated with submergence are not accounted for (Nielsen et al. 2022). Here, we present the first comprehensive assessment of shoreline change rates with respect to morphology for the entire Tuktoyaktuk Peninsula, analysing shoreline and coastal zones from orthorectified aerial and satellite imagery from 1950, 1985, and 2020 at very high resolution. The objectives of the study are to identify trends of shoreline change and to characterise the spatial patterns, discussing their controls.

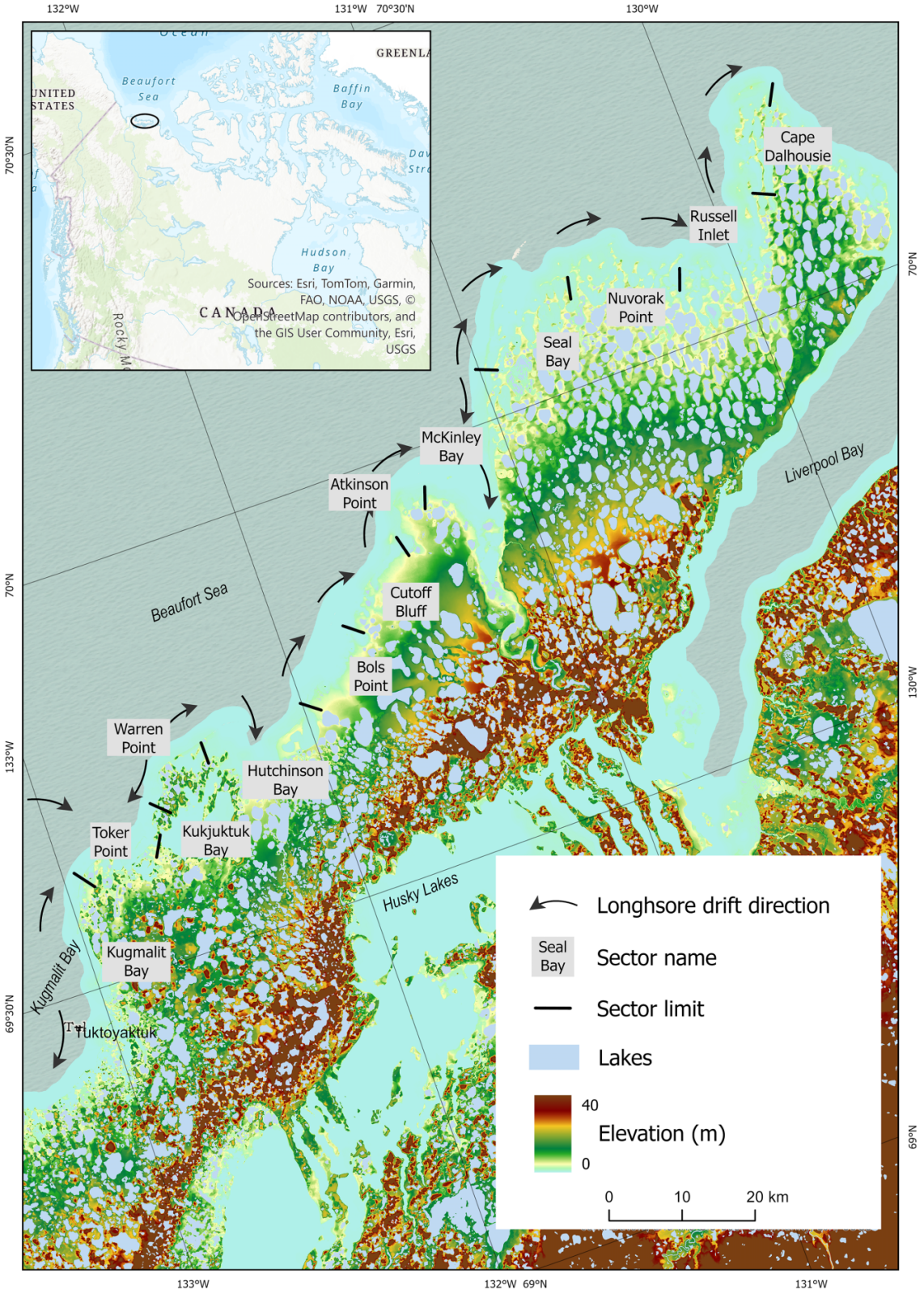
2. Study area

The Tuktoyaktuk Peninsula (69.4°N, 133.0°W) spans 1250 km^2 and is part of the Inuvialuit Settlement Region. It comprises Late Pleistocene-Holocene sediments with high ground ice content in continuous permafrost (Plug et al. 2008; Pelletier and Medioli 2014; Zwieback et al. 2018; Manson et al. 2019; Wolfe et al. 2020). The surficial geology is mainly composed of gravelly sands and sandy hills, ridges, and terraces alternated with thermokarst lake beds and barrier beaches (Rampton 1988). The Tuktoyaktuk Peninsula coastline transitions from lacustrine plains and glaciofluvial terraces with barrier beaches and large lagoons in the southwest (Tuktoyaktuk Hamlet to Kukjuktuk Bay), to glaciofluvial outwash plains and aeolian deposits with smaller thermokarst lakes and a more regular shoreline between Kukjuktuk Bay and McKinley Bay (Fig. 1). Northeast of McKinley Bay, extensive aeolian and lacustrine deposits are interspersed with large, SSW–NNE trending thermokarst lakes, whose breaching has produced a highly sinuous coastline with numerous peninsulas and bays (Rampton 1988; Pelletier and Medioli 2014; Wolfe et al. 2020; Whalen et al. 2022). It is characterised by low elevation (Fig. 1), dotted with thermokarst lakes and underlain by continuous permafrost, making it vulnerable to coastal submergence from sea level rise, inundation events, and permafrost thaw subsidence (Creel et al. 2024). Ground ice content is highest (>30%) in localised southwestern sectors (e.g., Toker Point), moderate (20%–30%) across much of the southwest, and decreases to 5%–20% in central and north-eastern areas (O'Neill et al. 2019, 2022; Wolfe et al. 2021).

Astronomical tides, wind-driven storm surges (Kim et al. 2021), and long-term relative sea-level rise (James et al. 2021) are the main drivers of water-level changes in the area, with northwesterly storms generating surges exceeding 2 m despite a minimal tidal range of 0.3–0.5 m; driftwood markers indicate the extent of historical flood events (Forbes et al. 2014; Kim et al. 2021; MacLeod and Dallimore 2021; Whalen et al. 2022). The Mackenzie River influences water properties, longshore currents, sediment distribution, and relative sea-level in the region (Pelletier and Medioli 2014). Water level is also driven by short-term seasonal sea-ice formation and melt (Manson and Solomon 2007; Trishchenko et al. 2022), and long-term climate-driven changes in temperature and sea ice (Barnhart et al. 2014*b*, 2016; Galley et al. 2016; Yang et al. 2023), as well as coastal erosion that may influence local hydrodynamics (Héquette et al. 2001; Forbes et al. 2014; Whalen et al. 2022). Alongshore currents mainly follow a SW–NE direction (Pelletier and Medioli 2014), and sea ice covers the coast for 7–8 months, with the ice-free period generally occurring from late June to October (Solomon 2005; Forbes et al. 2014; Ford et al. 2016). Sea-ice trends in the Beaufort Sea are changing, with delayed freeze-up extending the open-water season (Galley et al. 2016).

The hamlet of Tuktoyaktuk (c. 900 inhabitants), located in the southwestern part of the peninsula, faces persistent threats from coastal erosion, which has accelerated since 2000 despite protection efforts (Whalen et al. 2022). Tuktoyaktuk has a prevailing westerly wind, with notorious northwesterly storms which increase in strength and frequency in the late autumn before freeze-up (Solomon 2005; Manson and Solomon 2007; O'Rourke 2017; Trishchenko et al. 2022). Rising sea levels, permafrost thaw subsidence, and isostatic subsidence play an essential role in the changing coastal landscapes, particularly in low-lying areas around the hamlet. Relative sea-level rise of 2.5 mm/year from 1960 to 2020, projected to increase to 7.15 ± 1.1 mm/year after 2020, exacerbates these risks (Atkinson et al. 2016; Greenan et al. 2019; James et al. 2021), as it will also increase the frequency and magnitude of storm events (Lamoreux et al. 2015; Ford et al. 2018). The community also faces threats to travelling, subsistence activities, infrastructure, culture, and health (Irrgang et al. 2019; Brady and Leichenko 2020; Liew et al. 2020; Ramage et al. 2022; Whalen et al. 2022).

Fig. 1. The Tuktoyaktuk Peninsula and its main coastal sectors (from southwest to northeast): (1) Kugmalit Bay, (2) Toker Point, (3) Kukjuktuk Bay, (4) Warren Point, (5) Hutchinson Bay, (6) Bols Point, (7) Cutoff Bluff (Drift Point), (8) Atkinson Point, (9) McKinley Bay, (10) Seal Bay, (11) Nuvorak Point (Cape Brown), (12) Russell Inlet, and (13) Cape Dalhousie. Figure was created using ArcGIS Pro version 3.4.0 and assembled from the following data sources: Placenames were based on information from Canadian Toponymic Names and consultations with Tuktoyaktuk Elders–Inuvialuit names were used preferably, Longshore drift information was obtained from the Environmental Atlas of the Beaufort Coastlands (Pelletier and Medioli 2014), Lakes data obtained from CanVec Series–Hydrographic Feature. Elevation data was obtained from ArcticDEM v. 4.1 (Porter et al. 2023). Base map from ESRI, courtesy of ESRI, TomTom, USGS, Garmin, FAO, NOAA and OpenStreetMap contributors.



Arctic Science Downloaded from cdnsciencepub.com by ENR-ITILIBBF on 10/30/26

Fig. 2. Methodological approach for assessing the shoreline evolution of the Tuktoyaktuk Peninsula from 1950 to 2020.

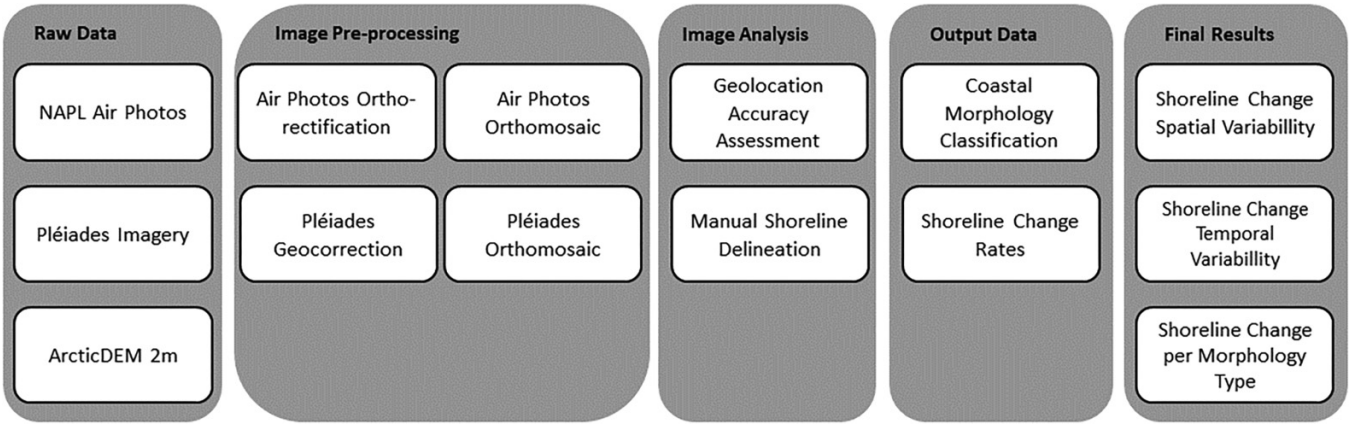


Table 1. Characteristics of satellite imagery and aerial photography.

Image type	Acquisition date	Number of scenes	Scale	Bands
Aerial photography (monochromatic)	14 July 1950	3	1:40 000	1
	15 July 1950	48		
	15 August 1950	14		
	22 August 1950	15		
	2 August 1985	3	1:60 000	
	3 August 1985	2		
	5 August 1985	1		
	6 August 1985	16		
CNES/Pléiades (multispectral, pansharpened)	12 July 2020	3	–	4
	24 July 2020	2		
	31 July 2020	2		

3. Methods

3.1. Introduction

We analysed shoreline change dynamics on the Tuktoyaktuk Peninsula by generating orthomosaics from 1950 and 1985 aerial photographs and co-registering them with VHR 2020 Pléiades satellite imagery. These datasets were subject to manual shoreline delineation and coastal morphology classification, and were used to derive shoreline change rates for three periods: 1950–1985, 1980–2020, and 1950–2020 (Fig. 2). Sectors present in figures and tables were defined according to geomorphological homogeneity and proximity to known toponyms. North-eastern sectors are more homogeneous and have fewer established toponyms.

3.2. Satellite and aerial photography, orthophotos, and image processing

The Pléiades satellite constellation, operated by CNES and Airbus Defence and Space, consists of two very high-resolution optical satellites (Pléiades-1A and 1B) launched in 2011 and 2012, providing 0.5 m panchromatic and 2 m multispectral imagery suitable for VHR remote sensing analyses (Gabriel-Robez et al. 2012; Almar et al. 2019; Diatta et al. 2025; Burvingt et al. 2025). Orthophotos were produced using 142 panchromatic aerial photographs from the Natural Resources Canada National Air Photo Library (Table 1). Where sufficient image overlap existed, photographs were processed into orthophotomosaics using PIX4Dmapper 4.8.4 by triangulating common tie points across all photographs, incrementally adding additional images through iterative re-optimization, and georeferencing the resulting mosaic using ground control points from ArcticDEM and 2020 Pléiades imagery. For images lacking overlap (24 from 1950 and all from 1985), individual orthophotos were generated using ENVI 5.6. This workflow involved constructing rational polynomial coefficients, correcting relief displacement and camera distortions using ArcticDEM, and refining georeferencing in QGIS using $\geq$25 GCPs per image. Final orthophotomosaics and orthophotos achieved resolutions of 0.48 m (1950) and 0.76 m (1985).

3.3. Accuracy assessment

The geolocation accuracy of the 2020 Pléiades satellite imagery was based on the RPC model without ground control points, using ArcticDEM 2 m as the elevation source. A root mean square error (RMSE) of 3 m was assumed, reflecting the typical horizontal positional uncertainty for RPC-only georeferencing (Burningham and Fernandez-Nunez 2020). To assess accuracy, we generated a 2500 m fishnet grid across the study

Arctic Science Downloaded from cdnsciencepub.com by ENR-ITILIBBF on 10/30/26

Table 2. Accuracy of aerial photography orthorectification, image geolocation positioning and shoreline uncertainty indexes.

Year	Ground resolution (m)	RMSE (m)	LOA (m)	Tidal effects	U_{sp} (m)
1950	0.48	2.43	2	0.3	3.20
1985	0.76	3.59	2	0.3	4.19
2020	0.51	3.00	2	0.3	3.65

Note: RMSE, root mean square error; LOA, loss of accuracy.

Table 3. Dilution of accuracy (DOA) for all studied periods.

Period	DOA (m/year)
1950–1985	0.15
1985–2020	0.16
1950–2020	0.07

area, sampling 1–2 random points per cell to ensure spatial representativeness and avoid clustering. Coordinates from all imagery dates (1950, 1985, and 2020) were compared, and shoreline position uncertainty (U_{sp}) was calculated as:

$$U_{sp} = \sqrt{GR_I^2 + RMSE^2 + LOA^2 + E_T^2}$$

where GRI is the ground resolution (Table 2), RMSE is the positional error, LOA is the assumed loss of accuracy of 2 m for the manually digitised shorelines, as used in other studies (Hapke and Reid 2007; Irrgang et al. 2018; Clark et al. 2021; Tanguy et al. 2023), and E_T is the tidal effects due to the use of the mean high-water line (MHWL from now on) as the shoreline proxy, as a proxy for horizontal shoreline variability (Boak and Turner 2005). Including E_T is justified because even small vertical tidal fluctuations can produce measurable horizontal shifts in the MHWL position on low-gradient Arctic coasts, and this approach is standard in shoreline change studies (Boak and Turner 2005; Irrgang et al. 2018).

The dilution of accuracy (DOA) quantifies the cumulative uncertainty in shoreline change rates by integrating positional errors from both time points in each period (Table 3). Calculated as:

$$DOA = \frac{\sqrt{{U_{sp1}}^2 + {U_{sp2}}^2}}{\Delta t}$$

where U_{sp1} and U_{sp2} are the shoreline position uncertainties for two of the studied years, and Δt is the timespan in years (Hapke and Reid 2007; Irrgang et al. 2018; Ward Jones et al. 2019; Cunliffe et al. 2019; Clark et al. 2021). It was integrated into each shoreline change rate period, and rates valued within the range of zero to DOA were deemed statistically insignificant (Table 3). These values are added to the shoreline change values to provide the uncertainty range for each period.

3.4. Coastal morphology classification

The coastal morphology was classified following a two-tier system after Couture et al. (2015), who divided the backshore and foreshore based on geomorphological and sedimentological characteristics. The classification was conducted by analysing the 2020 Pléiades satellite imagery, the ArcticDEM 2 m resolution, and the derived hillshade model at a scale of 1:1000. The backshore was divided into (1) bluffs with low ice-wedge degradation, (2) bluffs with high surface degradation, (3) tundra flats, and (4) barrier beaches and sandspits, further subdivided based on specific characteristics (Table 4, Fig. 3). The foreshore morphology was divided into (1) beach, (2) tundra flats, and (3) active bluffs (Table 4, Fig. 4). Solomon (2005) and Ford et al. (2016) provided a regional coastal context while Pelletier and Medioli (2014) offered detailed morphological descriptions. Bluff subdivisions by height and all foreshore classes were based on Couture et al. (2015). Backshore tundra flats and barrier beaches and sandspits were based on Pelletier and Medioli (2014), which also provided a basis for most backshore subclass definitions (Table 4).

3.5. Shoreline digitising and change rates calculation

A single operator manually digitised the shorelines for each year. The 1950 and 1985 shorelines were delineated at a constant digital scale of 1:500 to ensure consistency. The 2020 shoreline was digitised at a scale between 1:250 and 1:500 to capture maximum detail, allowing for its use in future VHR studies. To optimise shoreline comparison, integration in the digital shoreline analysis system (DSAS), and transect orientation, the 2020 shoreline was smoothed in ArcGIS to eliminate redundant angles and small variations.

Following studies on the Beaufort Sea coast, such as O'Rourke (2017), Radosavljevic et al. (2016), and Solomon (2005), the MHWL was selected as the shoreline proxy. This choice served two main purposes: firstly, it made for clearer discrimination of shoreline position in black-and-white aerial imagery from 1950 and 1985; secondly, it minimised the influence of tidal fluctuations on shoreline mapping (Boak and Turner 2005; Burningham and Fernandez-Nunez 2020). It also provides a better understanding of coastal morphodynamics and changes in coastal morphology compared to other criteria, such as the cliff top or the vegetation line, which fail to assess aggradation, sediment rebalance, and foreshore zone changes.

Shoreline positions derived from 2020 imagery dated 31 July correspond to areas affected by an ongoing storm surge and were therefore digitised along the instantaneous water line, which lay above the mean high-water line (MHWL). The surge-affected sectors (KUG, TOKR, KUKJ, and WARR) represent approximately 2/7 of the study area. In those cases the water line was conservatively interpreted as the high-water line for rate calculations, given that the MHWL was not observable. For imagery from 12 and 24 July, acquired during low tide, the MHWL was used as the shoreline proxy except in sectors with snow or ice on the beach or at the bluff base, as seen in 7.6% (48 km) of the study area in 2020,

Arctic Science Downloaded from cdnsciencepub.com by ENR-ITILIBBF on 10/30/26

Table 4. Description of the coastal morphology classification system used for the Tuktoyaktuk Peninsula (Figs. S1 and S2).

	Class	Subclass	Definition
Backshore	Bluffs with low surface degradation	Very low height	Unconsolidated vertical or sloping bluffs exposed to subaerial and marine weathering (0.5–2 m high), with the absence of ice-wedge polygons or minimal to low degradation in ice-wedge polygons.
		Low height	Unconsolidated, vertical, or sloping, exposed to subaerial and marine weathering (2–5 m high), with the absence of ice-wedge polygons or minimal to low degradation in ice-wedge polygons.
		Medium height	Unconsolidated vertical or sloping bluffs exposed to subaerial and marine weathering actions (5–15 m high), with the absence of ice-wedge polygons or minimal to low degradation in ice-wedge polygons.
		Slump toe bluff	Complex coastal bluffs with active or relict landslides.
	Bluffs with high surface degradation	Very low height	Unconsolidated vertical or sloping bluffs, exposed to subaerial and marine weathering (0.5–2 m high), with evident signs of degradation in ice-wedge polygons.
		Low height	Unconsolidated, vertical, or sloping, exposed to subaerial and marine weathering (2–5 m high), with evident signs of degradation in ice-wedge polygons.
		Medium height	Unconsolidated vertical or sloping bluffs, exposed to subaerial and marine weathering actions (5–15 m high), with evident signs of degradation in ice-wedge polygons.
	Tundra flats	Inundated flats and polygons	Submerged low-relief tundra flats extending into the nearshore and foreshore as a result of sea-level rise, with complex and crenellated coastlines; foreshore beaches are usually non-existent or narrow; organic-rich areas are common.
		Intertidal flats with wetlands	Periodically submerged low-relief tundra with lakes associated with wetlands and complex embayments formed by the breaching of thermokarst lake basins; flats are often wide (>200 m), the coastlines are complex and highly crenellated, without beaches and with wide intertidal flats with the presence of intertidal lakes in the foreshore zone; organic-rich areas are common.
	Barrier beaches and sandspits		Sandy to gravelly beach formations showing variable width and low relief, influenced by wave exposure and longshore drift. Backshore dune formations may be present.
Foreshore	Beaches		Sandy to gravelly beaches, deposited by longshore currents fronting any backshore unit.
	Tundra flats		Submerged tundra flats without sedimentary cover.
	Active bluffs		Unconsolidated vertical or sloping bluff sediments are exposed to subaerial and marine weathering actions without a beach during high tide. Very sensitive to thermal abrasion and wave forcing.

the bluff top was used as a shoreline proxy across all dates (Fig. S3).

Shoreline change rates were computed in ESRI's ArcMap software 10.8, using the DSAS v5.0 (Himmelstoss et al. 2018; Irrgang et al. 2018; Zagórski et al. 2020; Bartsch et al. 2020; Buzard et al. 2023; Tanguy et al. 2023). A baseline parallel to the 2020 shoreline was drawn offshore and adjusted to ensure alignment with the shorelines at all three dates. Transects were spaced at 50 m intervals and adjusted for optimal perpendicularity and to ensure optimal orientation, following (Hapke and Reid 2007). The linear regression rate (LRR) was used to calculate change rates in the 1950–2020 period. LRR fits a linear regression model to the shoreline intersections for each transect, with the slope representing the shoreline trend. This rate represents a time-averaged trend, assuming a linear model that best fits the full set of shoreline positions (Himmelstoss et al. 2018; Burningham and Fernandez-Nunez 2020). The end point rate (EPR) was used to calculate change rates in the 1950–1985 and 1985–2020 periods, where shoreline retreat is expressed as negative values, and positive values indicate advance (Himmelstoss et al. 2018; Burningham and Fernandez-Nunez 2020).

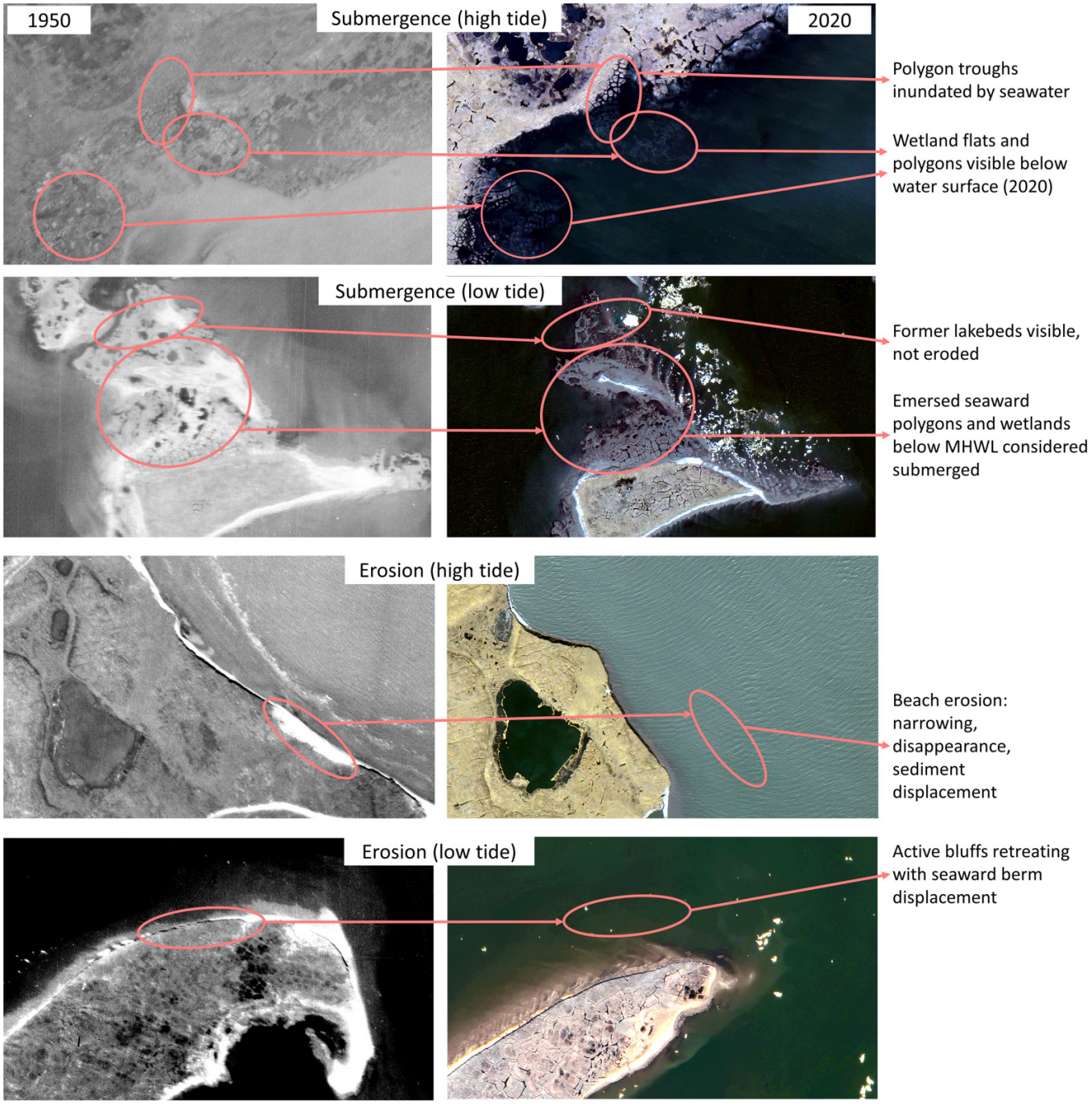
3.6. Submergence and erosion in coastal process identification

Coastal processes were identified through a comparative assessment of submergence and erosion indicators across the three analysed years. The MHWL was the chosen shoreline proxy, defining the seaward land limit (see 3.5.). Process identification relied on the visual interpretation of shoreline change in coastal morphologies, using orthomosaics derived from aerial photographs for 1950 and 1985, as well as VHR Pleiades satellite imagery for 2020. Because tidal conditions varied across the Pleiades acquisitions, with two of the seven orthomosaics taken during high-tide conditions and the remaining five during low-tide conditions, the coastal process was documented for each tidal stage to maintain proxy consistency and ensure accurate process identification for each tidal condition. This ensured transparency and reproducibility in future coastal-change research based on similar VHR datasets.

Submergence was defined as the loss of previously exposed coastal areas due to progressive inundation caused by permafrost thaw subsidence and sea-level rise. High-tide imagery revealed submergence in low-lying tundra flats, polygonal

Arctic Science Downloaded from cdnsciencepub.com by ENR-ITILIBBF on 10/30/26

Fig. 3. Example cases of identifying coastal submergence and coastal erosion processes, observed across different tidal states at the time of the 2020 Pléiades satellite imagery (1950–2020). Base map: Orthorectified NAPL aerial photography © NRCan (left) and 2020 Pléiades satellite imagery: PLEIADES © CNES, 2020, distribution Airbus DS (right).

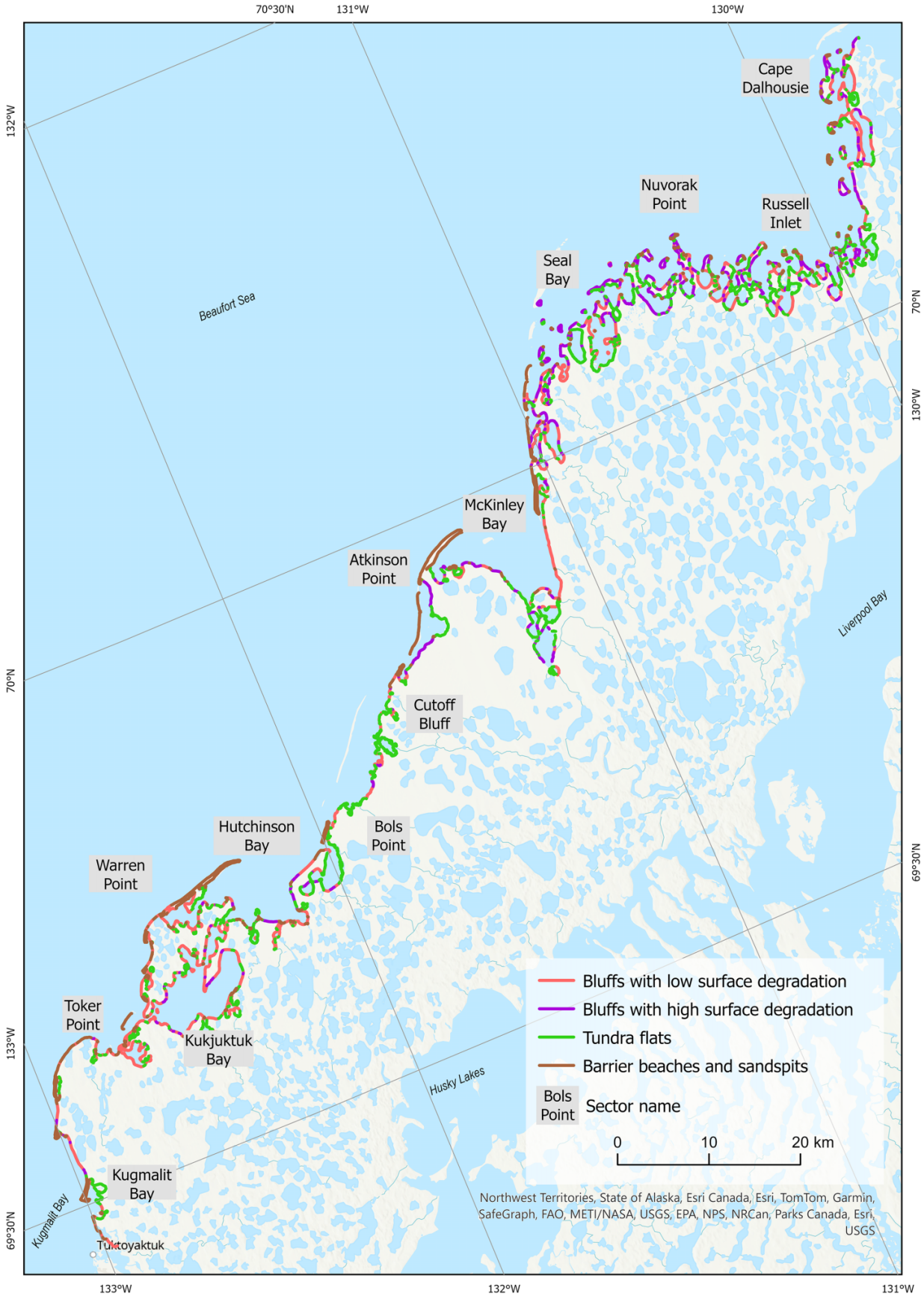


Arctic Science Downloaded from cdnsciencepub.com by ENR-ITILIBBF on 10/30/26

tundra structures, ice-wedge troughs, wetlands, salt marshes, and barrier beaches (to a lesser extent). These features provided clear visual cues when their morphology was submerged, such as emerged tundra polygons with adjacent features visible underwater, confirming progressive inundation (Fig. 3). Low-tide mosaics reinforced these observations, showing tundra flats, wetlands, and polygon areas that, although still emerged, lay below the MHWL threshold or were visibly submerged with clear, identifiable features. Therefore, the consistency of these observations across both tidal states indicated transgressive processes, particularly in low-lying tundra flats and wetlands, which evolved into intertidal zones.

Erosion was defined as the mass removal or redistribution of soil, ground or sediment. In high-tide mosaics, erosion was visible through beach narrowing or disappearance, beach berm displacement, and bluff retreat from bottom or top (thermo-denudation or thermo-abrasion (Günther et al. 2013) (Fig. 3). Variability in bluff degradation ranged from intact but retreating frontages to heavily undercut margins where polygonal cliff faces collapsed. Low-tide imagery con-

Fig. 4. Backshore coastal morphology of Tuktoyaktuk Peninsula. Figure was created using ArcGIS Pro version 3.4.0 and assembled from the following data sources: Placenames were based on information from Canadian Toponymic Names and consultations with Tuktoyaktuk Elders–Inuvialuit names were used preferably. Base map from ESRI, courtesy of the named organizations.



Arctic Science Downloaded from cdnsciencepub.com by ENR-ITILIBBF on 10/30/26

Table 5. Coastal morphology proportion of each class and subclass in the Tuktoyaktuk Peninsula.

	Class	Coverage (%)	Subclass	Coverage (%)
Backshore	Bluffs with low surface degradation	42	Very low	22
			Low	15
			Medium	4
			Slump toe bluff	0.4
	Bluffs with high surface degradation	15	Very low	12
			Low	3
			Medium	0.1
	Tundra flats	28	Inundated flats and polygons	21
			Intertidal flats with wetlands	7
	Barrier beaches and sandspits	15		
Foreshore	Beaches	53		
	Tundra flats	31		
	Active Bluffs	16		

Arctic Science Downloaded from cdnsciencepub.com by ENR-ITILIBBF on 10/30/26

firmed these patterns, showing sediment displacement, reduced beach volumes, berm shifts, and further bluff retreat relative to 1950 and 1985. In some cases, slumps driven by thermo-denudation provided additional indicators of erosional activity.

Certain environments showed spatial coexistence of submergence and erosion processes. In tundra polygons, former thermokarst lake margins, tidal flats, and small bluffs (below 0.5 m), submergence dominated through progressive inundation and permafrost thaw subsidence, with apparent RSL rise contributing to observed changes. Erosion played a secondary role, particularly in sheltered areas where submerged features remained visible. Wetland fringes at intertidal flat edges exemplified this, combining progressive inundation with sediment redistribution. While barrier beaches also exhibited submergence patterns (if located in the same areas), in most observations, we found a higher influence of erosion in these landforms.

Therefore, shoreline retreat reflected varying controls depending on coastal morphology. Submergence dominated shoreline retreat in foreshore and backshore tundra flats, while erosion dominated in foreshore beaches, backshore and active bluffs and barrier beaches and sandspits. Aggradation was observed as shoreline advance compared to previous years, primarily driven by morphodynamic processes such as beach progradation through sediment redistribution and deposition in the foreshore zone. The MHWL was selected over other proxies to facilitate the assessment of these morphodynamic changes.

By applying clear, rule-based criteria across multiple tidal states, timeframes, and a detailed VHR coastal morphology classification, this approach produced a systematic classification of dominant coastal retreat processes (submergence vs. erosion) that influenced shoreline evolution between 1950 and 2020. This record provides the basis for evaluating long-term shoreline dynamics and supports our interpretation of coastal change in the Tuktoyaktuk Peninsula.

4. Results

4.1. Coastal morphology

Tuktoyaktuk Peninsula shows 41% of its backshore as bluffs with low surface degradation (22% very low, 15% low, 4% medium, and 0.4% slump toe bluffs). Tundra flats comprise 28% of the area, with 21% identified as inundated tundra flats and polygons and 7% as intertidal inundated flats with wetlands. Bluffs with high surface degradation (12% very low, 3% low, and 0.1% medium) cover 15% of the coast, while barrier beaches and sandspits account for an additional 15%. Concerning the foreshore morphology, beaches occupy 53% of the shoreline, while tundra flats represent 31%, and active bluffs comprise 16% of the study area (Table 5).

The backshore can be categorised into five main areas (Fig. 4):

Kugmalit Bay to Warren Point features barrier beaches and sandspits along with higher bluffs (>2 m height) with low surface degradation.

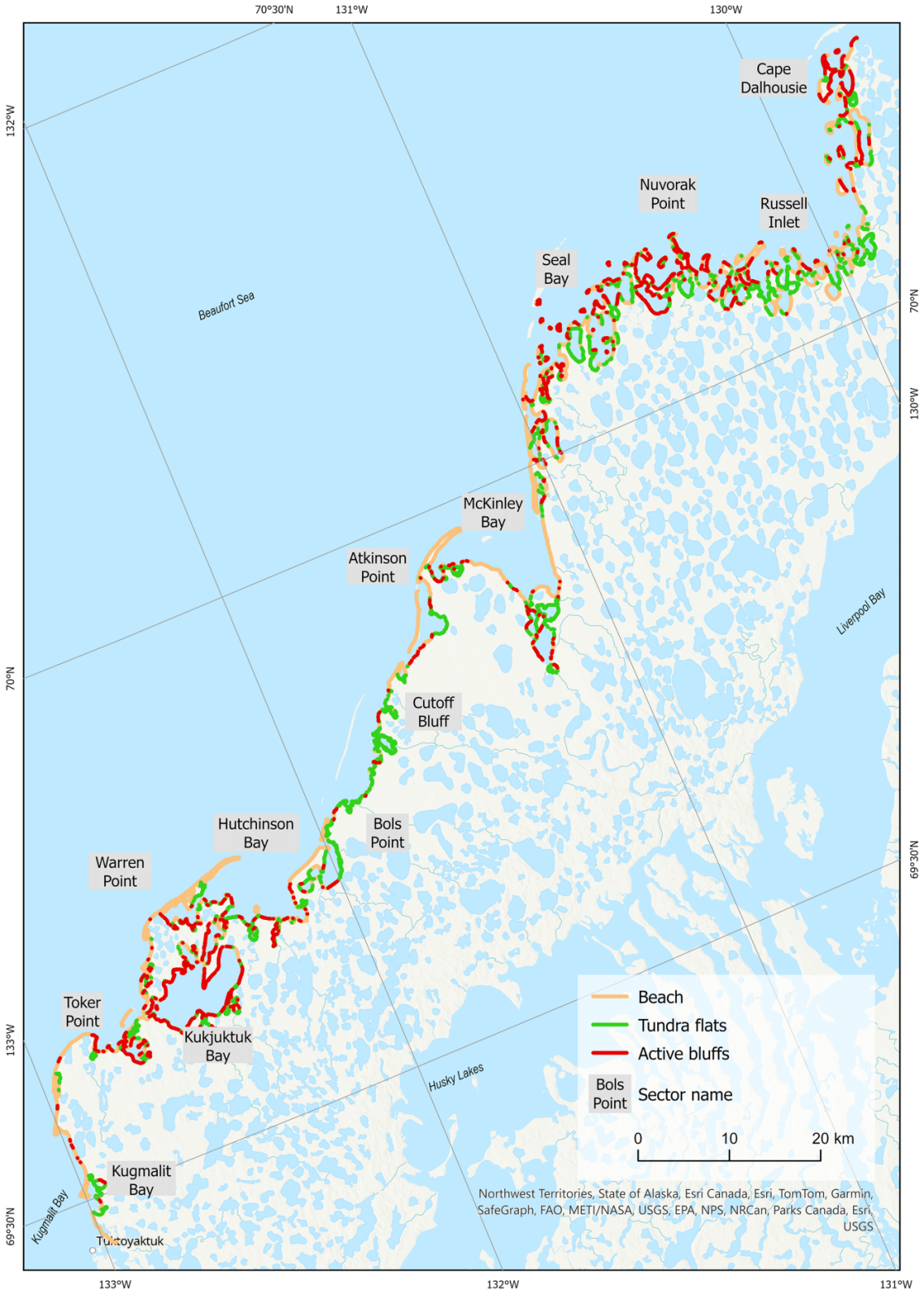
Hutchinson Bay to Atkinson Point is characterised by a high concentration of tundra flats and lower bluffs (<2 m height) with high surface degradation.

Seal Bay to Russell Inlet exhibits a similar coastal configuration marked by shoreline sinuosity, resulting from the erosion of former thermokarst lakes and lagoons that have formed multiple bays and peninsulas. This region has a higher concentration of lower bluffs with high surface degradation, located in exposed areas, while tundra flats are found in sheltered areas.

McKinley Bay and Cape Dalhousie are two transitional sectors with lower shoreline sinuosity, featuring bluffs with low surface degradation in exposed areas and tundra flats in sheltered areas.

Foreshore morphology is primarily beaches (Fig. 5). Tundra flats are concentrated east of Hutchinson Bay, while active bluffs are found in both sheltered (e.g., Kukjuktuk Bay)

Fig. 5. Foreshore Coastal Morphology Classification in the Tuktoyaktuk Peninsula. Figure was created using ArcGIS Pro version 3.4.0 and assembled from the following data sources: place names were based on information from Canadian Toponymic Names and consultations with Tuktoyaktuk Elders–Inuvialuit names were used preferably. Base map from ESRI, courtesy of the named organizations.



and exposed areas beyond McKinley Bay. The relationship between backshore and foreshore classes reveals that bluffs with low surface degradation are mostly fronted by foreshore beaches (60%), have no foreshore and are therefore active bluffs (28%), or, occasionally, are fronted by tundra flats (11%), usually in areas with minimal bluff height (0.5–1 m).

Arctic Science Downloaded from cdnsciencepub.com by ENR-ITILIBBF on 10/30/26

Table 6. Percentage of backshore classes fronted by each foreshore morphology (by % area).

Backshore	Foreshore		
	Beach	Tundra flats	Active Bluffs
Bluffs with low surface degradation	60	11	29
Bluffs with high surface degradation	54	14	32
Tundra flats	16	84	0
Barrier beaches and sandspits	100	0	0

Table 7. Shoreline change statistics for the Tuktoyaktuk Peninsula and each period analysed.

Period	Mean shoreline change rate (m/year)	Median shoreline change rate (m/year)	Retreat (% of all transects)	Retreat ≤−1 m/year (% of all transects)	Aggradation (% of all transects)	Aggradation ≥1 m/year (% of all transects)
1950–1985	−0.67	−0.45	85	26	15	3
1985–2020	−0.88	−0.56	91	29	9	3
1950–2020	−0.77	−0.53	94	27	6	1

Arctic Science Downloaded from cdnsciencepub.com by ENR-ITILIBBF on 10/30/26

Where tundra flats front bluffs, these are generally backshore tundra highlands or slopes affected primarily by permafrost thaw and subsidence and progressive inundation and submergence, rather than direct wave undercutting. Bluffs with high surface degradation exhibit similar patterns to those with low surface degradation, although with a slightly higher frequency of tundra flats in the foreshore (14%). Beaches also mostly front these landforms (54%), and active bluffs represent 32% (Table 6). Tundra flats in the backshore predominantly continue as tundra flats in the foreshore (84%) and are seldom fronted by beaches (16%). Lastly, as expected, barrier beaches and sandpits are always fronted by foreshore beaches.

4.2. Shoreline change rates and patterns

4.2.1. Shoreline changes from 1950 to 2020 and its temporal variability

Shoreline change rates from 1950 to 2020 along the 633 km of coast in the Tuktoyaktuk Peninsula yielded an average of -0.77 ± 0.07 m/year, with 94% of the area displaying shoreline retreat (Table 7). 27% of the coast showed values equal to or lower than −1 m/year, while 6% of the coast was aggrading, with 1% exceeding 1 m/year. Approximately 45% of the coast exhibited change rates between −0.5 and 0.5 m/year, while 7% displayed minor changes within the DOA. The absolute change rates ranged from -26.1 ± 0.07 m/year in tundra flats to 7.6 ± 0.07 m/year in barrier beaches and sandspits, highlighting significant variability of shoreline evolution.

Shoreline change rates increased from 1985–2020 compared to 1950–1985 (Table 7). The mean shoreline change rate rose from -0.67 ± 0.15 m/year to -0.88 ± 0.16 m/year, while the median increased from −0.45 m/year to −0.56 m/year. The spatial extent of shoreline retreat expanded, with 85% of the coast retreating in the earlier period and 91% in the later period. Transects with retreat rates of −1 m/year or higher increased from 26% to 29% between the two periods. Aggradation above 1 m/year remained minimal at 3% in both periods. Approximately 44% of the coast experienced an acceleration in retreat rates. When combined with areas that shifted from aggradation to retreat, this constituted the majority, 56% of the coast. About 13% transitioned from aggradation to retreat between the two periods. Conversely, 36% experienced deceleration in retreat, and 5% shifted from retreat to aggradation. A small proportion showed changes in aggradation rates, with 0.8% decelerating and 0.7% accelerating, indicating minimal shoreline progradation. Only 1.1% of the study area displayed no significant change, within zero and the DOA values in m/year. These trends reflect long-term averages and may have potentially averaged out short-term, episodic changes that contributed to increased rates.

The shoreline retreat expanded from 85% (1950–1985) to 91% (1985–2020) of the coast. Concurrently, aggradation decreased from 15% to 9% of transects. Retreat rates exceeding −1 m/year corresponded to 26% of the coast from 1950 to 1985 and 29% from 1985 to 2020, while aggradation ≥1 m/year remained limited to 3% of transects in both periods. Approximately 44% of the coast showed a retreat rate acceleration. The area with acceleration in retreat or that shifted from aggradation to retreat represented most of the coast (56%). About 13% of the area transitioned from aggradation in 1950–1985 to retreat during 1985–2020. Conversely, about 36% experienced deceleration in retreat, and 5% transitioned from retreat to aggradation. A small proportion of the area (0.8%) showed a deceleration in aggradation, and 0.7% recorded an acceleration in aggradation, indicating an overall minimal shoreline progradation pattern in the Tuktoyaktuk Peninsula. Lastly, 1.1% of the study area displayed no significant change. It is important to acknowledge that both periods are large, as short-term episodic changes are averaged and may have contributed to increased rates.

4.2.2. Spatial variability in the shoreline change rates

Shoreline change rates in the Tuktoyaktuk Peninsula from 1950 to 2020 showed retreat across all sectors, with mean rates from -0.50 ± 0.07 m/year to -1.55 ± 0.07 m/year

Table 8. Shoreline change statistics for the different sectors of Tuktoyaktuk Peninsula (1950–2020).

Sectors	Shoreline length (km)	Ground ice content	Mean change rate (m/year)	Median change rate (m/year)	Standard deviation	RT (%)	RT ≤ −1 m/year (%)	AG (%)	AG ≥ 1 m/year (%)
KUG	23.95	High	−0.98	−0.74	1.35	91	34	9	1
TOKR	42.6	High	−0.66	−0.33	0.95	91	26	9	3
KUKJ	53.8	High	−0.50	−0.40	0.42	98	10	2	0
WARR	29.9	Medium	−0.50	−0.33	0.86	84	16	15	2
HUTC	50.4	Medium	−1.11	−0.89	1.41	90	45	10	3
BOLS	19.75	Low	−1.23	−0.85	1.38	83	48	16	1
CUTO	16.6	Low	−1.36	−1.35	1.11	93	66	7	2
ATKN	12.55	Low	−1.55	−0.99	1.42	97	49	3	1
MCKN	72	Low	−0.81	−0.73	0.86	93	37	7	3
SEAL	81	Low	−0.71	−0.54	0.67	97	24	3	0
NUVR	110	Low	−0.61	−0.43	1.19	94	14	5	0
RUSS	66	Medium	−0.88	−0.75	0.74	97	36	3	0
DALH	54.1	Medium	−0.54	−0.37	0.69	97	14	3	1

Note: Sectors are abbreviated: KUG–Kugmalit Bay, TOKR–Toker Point, KUJK–Kukjuktuk Bay, WARR–Warren Point, HUTC–Hutchinson Point, BOLS–Bols Point, CUTO–Cutoff Bluff/Drift Point, ATKN–Atkinson Point, MCKN–McKinley Bay, SEAL–Seal Bay, NUVR–Nuvorak Point/Cape Brown, RUSS–Russell Inlet, DALH–Cape Dalhousie. Ground ice content information retrieved from (O'Neill et al. 2022).

Arctic Science Downloaded from cdnsciencepub.com by ENR-ITILIBBF on 10/30/26

(Table 8). Retreating patterns are widespread, affecting at least 83% of the shoreline in each sector, while aggradation occurred in only up to 16% of the coast. All sectors display a proportion higher than 14% of retreat higher than or equal to 1 m/year, with significant spatial variations. Conversely, areas over 1 m/year aggradation are residual among sectors.

In general, shoreline retreat was higher in sheltered areas despite hotspots in exposed areas facing the prevailing north or northwestern winds or with higher fetch areas (Fig. 6). Four sectors registered average retreat rates above −1 m/year: Hutchinson Bay, Bols Point, Cutoff Bluff (Drift Point) and Atkinson Point (Table 8). In these areas, tundra flats and very low bluffs with high surface degradation control the retreat rates. Also, the latter three sectors have large areas that are more exposed to the predominant winds in extreme weather events.

Sectors with lower average retreat rates also experienced a higher overall retreat rate due to extremely fast or fast retreat hotspots, especially those facing north or northeast, such as Toker Point, Warren Point, and McKinley Bay. Beyond McKinley Bay, sectors showed a consistent pattern of slow average retreat up to −1 m/year. Two types of hotspots emerged: areas exposed to prevailing winds and sheltered locations in bays formed by the breaching of former thermokarst lakes (Fig. 6). There is no evidence of storm surges or high surface wave heights affecting these results, as the 2020 imagery was captured during low tide, verified in the Tuktoyaktuk tidal station.

Sheltered sectors, such as Kukjuktuk Bay and Cape Dalhousie, characterised by bluffs without ice-wedge degradation, were more stable, with lower average retreat rates and less variable shoreline evolution. In contrast, Atkinson Point had the fastest average retreat (−1.55 ± 0.07 m/year) despite having a stable or slowly aggrading sandspit. Bols Point, Atkinson Point, and Cutoff Bluff showed similar rate distributions, with larger interquartile ranges indicating a greater influence of retreat rates above −1 m/year (Table 8, Fig. 7). Kugmalit Bay and Hutchinson Point also display a similar data distribution pattern (HUTC has a higher average retreat rate than KUG), despite the differences in location, predominant coastal orientation and general coastal morphology.

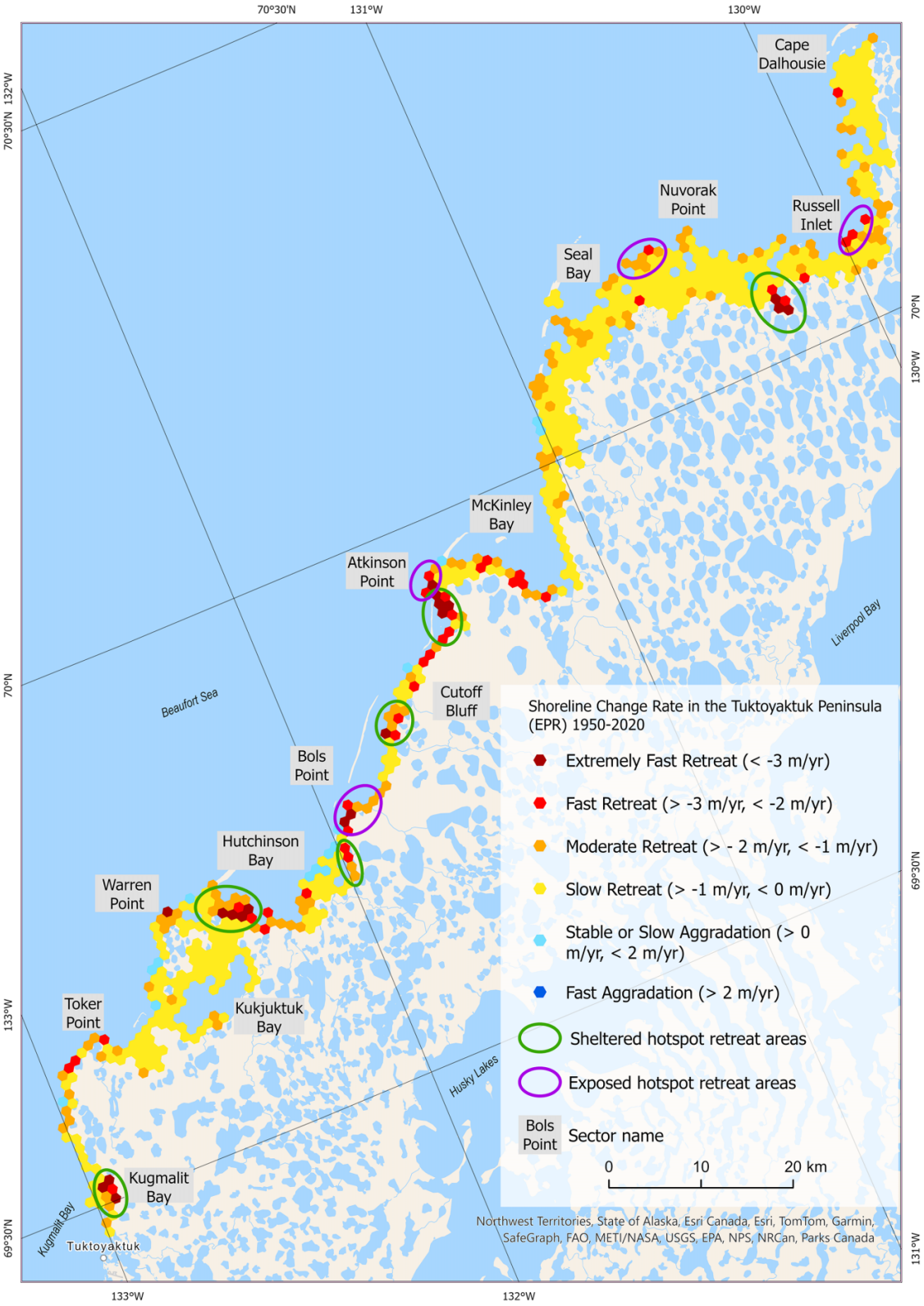
4.2.3. Coastal morphology and shoreline change rates: spatial and temporal variability

Shoreline change rates in the Tuktoyaktuk Peninsula varied significantly across different coastal morphologies. In the foreshore, tundra flats exhibited the highest average retreat rate of −1.01 ± 0.07 m/year, followed by beaches (–0.74 ± 0.07 m/year) and active bluffs (–0.62 ± 0.07 m/year), both below the overall mean retreat rate of –0.77 ± 0.07 m/year for 1950–2020 (Table 9). In the backshore, tundra flats also showed the highest average retreat at −1.09 ± 0.07 m/year, followed by bluffs with high surface degradation (−0.87 ± 0.07 m/year) and bluffs with low surface degradation (−0.60 ± 0.07 m/year). Barrier beaches and sandspits retreated at an average rate of −0.77 ± 0.07 m/year.

When examining the backshore morphology in detail, intertidal inundated flats with wetlands (–1.46 ± 0.07 m/year) and tundra flats and polygons (–0.98 ± 0.07 m/year) showed the greatest retreat, underscoring the vulnerability of tundra flats to shoreline retreat (Table 9). Very low bluffs with high surface degradation (−0.94 ± 0.07 m/year), barrier beaches and sandspits (−0.77 ± 0.07 m/year), and very low bluffs with low surface degradation (−0.72 ± 0.07 m/year) complete the five backshore landforms showing the highest shoreline change, indicating that low bluff height may be a factor which promotes shoreline retreat in the Tuktoyaktuk Peninsula. Slump toe bluffs (−0.70 ± 0.07 m/year), medium bluffs with low surface degradation (−0.53 ± 0.07 m/year), low bluffs with low surficial degradation (−0.47 ± 0.07 m/year), and medium bluffs with high surface degradation (−0.22 ± 0.07 m/year) are the units which display less retreat.

Retreat rates accelerated across all morphology units from 1950–1985 to 1985–2020. On the foreshore, tundra flats dis-

Fig. 6. Shoreline change rates in the Tuktoyaktuk Peninsula from 1950 to 2020. Figure was created using ArcGIS Pro version 3.4.0 and assembled from the following data sources: place names were based on information from Canadian Toponymic Names and consultations with Tuktoyaktuk Elders–Inuvialuit names were used preferably. Base map from ESRI, courtesy of the named organizations.



played the largest retreat acceleration, with an 87% increase from −0.71 ± 0.15 m/year (1950–1985) to −1.33 ± 0.16 m/year (1985–2020), along with the largest difference in median value and interquartile range (Fig. 8). Variability and dispersion also increased significantly (Table 10), as indicated by the rise in standard deviation (1.47–2.31) and VMR (−3.06

Arctic Science Downloaded from cdnsciencepub.com by ENR-ITILIBBF on 10/30/26

Fig. 7. Variability of shoreline change rates in the coastal sectors of Tuktoyaktuk Peninsula (1950–2020).

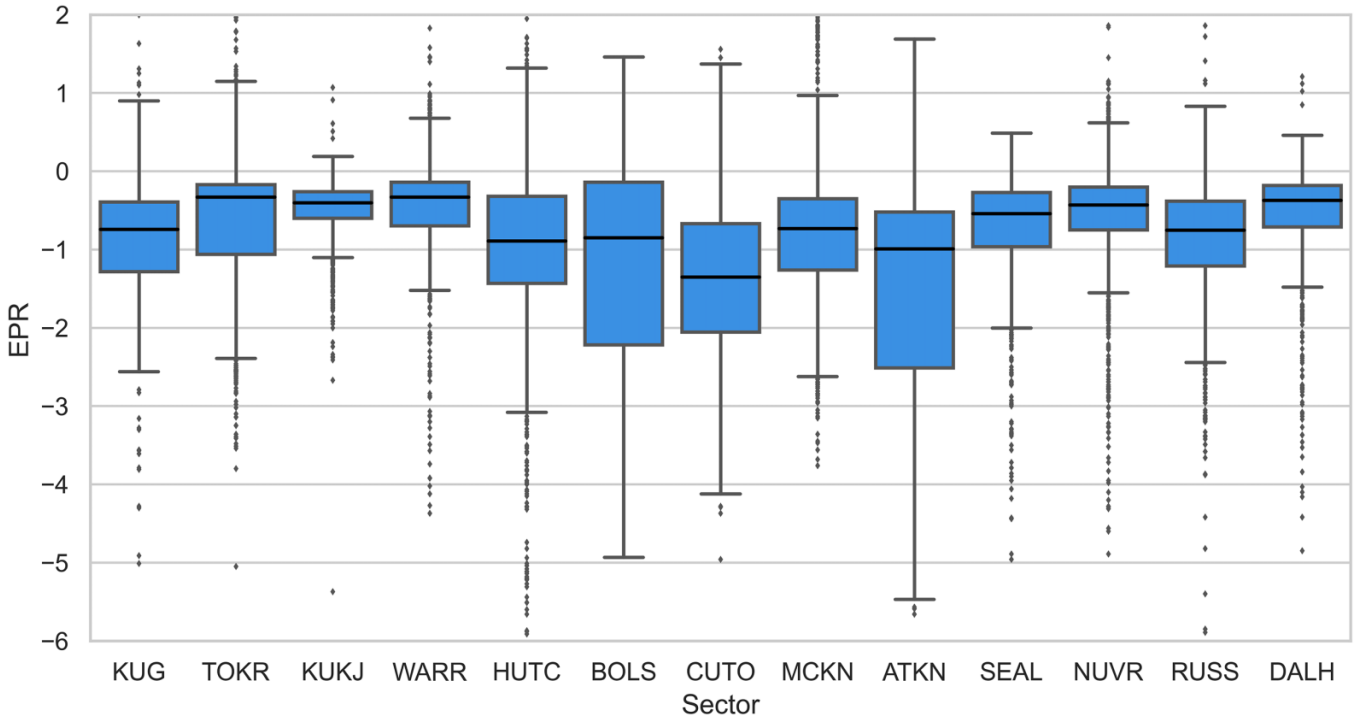


Table 9. Average shoreline change rates per coastal morphology class in the Tuktoyaktuk Peninsula (1950–2020).

	Coastal morphology class	EPR (m/year)
Backshore	**Tundra flats**	**−1.09**
	> Intertidal inundated flats with wetlands	−1.46
	> Tundra flats and polygons	−0.98
	Bluffs with high surface degradation	**−0.87**
	> Very low bluffs with high surface degradation	−0.94
	> Low bluffs with high surface degradation	−0.64
	> Medium bluffs with high surface degradation	−0.22
	Bluffs with low surface degradation	**−0.60**
	> Very low bluffs with low surface degradation	−0.72
	> Medium bluffs with low surface degradation	−0.53
	> Low bluffs with low surface degradation	−0.47
	> Slump toe bluffs	−0.70
	Barrier beaches and sandspits	**−0.77**
Foreshore	**Tundra flats**	**−1.01**
	Beaches	**−0.74**
	Active bluffs	**−0.62**

Note: EPR, end point rate. The bold texts are Backshore tundra classes, and the non bold classes are Detailed Backshore Tundra Classes.

to −4.01). Active bluffs experienced moderate acceleration, with rates increasing by 27%, from −0.55 ± 0.15 m/year to −0.70 ± 0.16 m/year, along with reduced variability and dispersion, as shown by the narrower interquartile range and lower VMR values. Foreshore beaches were the most stable landform in trends as they exhibited minimal change in median and mean rates, with retreat increasing slightly (13%) from −0.70 ± 0.15 m/year to −0.79 ± 0.16 m/year. Variability and dispersion increased slightly (Table 10), despite the lower interquartile range in the latter period.

In the backshore, bluffs with low surface degradation accelerated by 20% (–0.55 ± 0.15 m/year to –0.66 ± 0.16 m/year), while having the lowest median retreat values and maintaining low variability, the smallest interquartile range, a compact distribution and minimal changes in variance metrics across both periods (Table 10). Bluffs with high surface degradation showed minimal acceleration (6%). This class had the highest median retreat value during 1950–1985, although minimal changes in median values and interquartile range were observed over time. The data spread was slightly broader than for low-degradation bluffs, indicating marginally higher dispersion. Backshore tundra flats accelerated by 56% (–0.85 ± 0.15 m/year to –1.33 ± 0.16 m/year), with increased variability and dispersion, despite similar median and interquartile range values across periods. Barrier beaches and sandspits had the greatest acceleration among backshore classes (93%), with retreat rates nearly doubling and the largest interquartile range, reflecting high variability and retreat acceleration trends. Overall, tundra flats and barrier beaches and sandspits demonstrated higher retreat acceleration.

5. Discussion

5.1. Regional shoreline change trends

Shoreline change analysis for the Tuktoyaktuk Peninsula (1950–2020) revealed an average retreat rate of –

Arctic Science Downloaded from cdnsciencepub.com by ENR-ITILIBBF on 10/30/26

Fig. 8. Boxplots of shoreline change rates (m/year) per coastal morphology classes in the two studied periods: 1950–1985 (blue) and 1985–2020 (red). Backshore classes are represented to the left, and foreshore classes are represented to the right, separated by the dashed line for clarity.

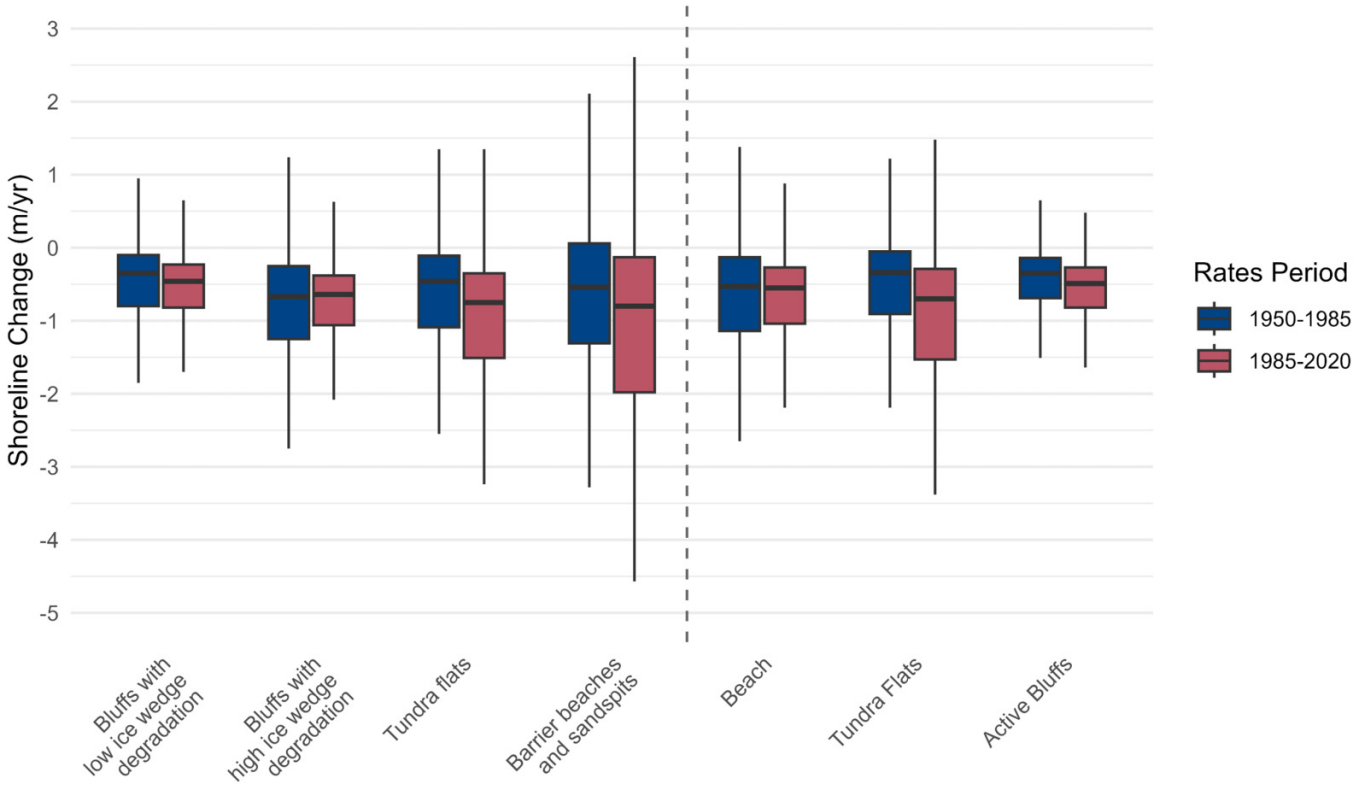


Table 10. Shoreline change rates variability and dispersion by backshore and foreshore class and period in the Tuktoyaktuk Peninsula (1950–2020).

	Class	Period	Average change rate (m/year)	Standard deviation	Variance to mean ratio (VMR)
Backshore	Bluffs with low surface degradation	1950–1985	−0.55	0.83	−1.26
		1985–2020	−0.66	1.06	−1.72
	Bluffs with high surface degradation	1950–1985	−0.86	0.90	−0.95
		1985–2020	−0.91	1.06	−1.23
	Tundra flats	1950–1985	−0.88	1.47	−2.55
		1985–2020	−1.33	2.25	−3.80
	Barrier beaches and sandspits	1950–1985	−0.53	1.72	−5.57
		1985–2020	−1.02	1.86	−3.40
Foreshore	Beaches	1950–1985	−0.70	1.08	−1.66
		1985–2020	−0.79	1.27	−2.05
	Tundra flats	1950–1985	−0.71	1.47	−2.55
		1985–2020	−1.33	2.31	−4.00
	Active bluffs	1950–1985	−0.55	0.77	−1.07
		1985–2020	−0.70	0.79	−0.89

0.77 ± 0.07 m/year, comparable to the Yukon Coast (−0.7 m/year), despite being characterised by the predominance of higher bluffs in the Yukon (Irrgang et al. 2018; Manson et al. 2019; O'Neill et al. 2022). This also aligns with the Alaskan Beaufort coast, where studies report erosion rates ranging from −0.7 to −2.4 m/year, despite a longer open water season in Alaska (Jones et al. 2009; Irrgang et al. 2018; Cunliffe et al. 2019). Extreme retreat rates reached −26.1 ± 0.07 m/year at low-lying tundra flats, consistent with Alaskan observations of −25 m/year in similar inundated tun-

Arctic Science Downloaded from cdnsciencepub.com by ENR-ITILIBBF on 10/30/26

Arctic Science Downloaded from cdnsciencepub.com by ENR-ITILIBBF on 10/30/26

dra (Gibbs and Richmond 2017), while accretion rates calculated (7.6 ± 0.07 m/year) at sandspits. The use of VHR imagery minimised uncertainty, with only 1.1% of transects showing non-significant changes (within DOA thresholds).

5.2. Spatial variability of shoreline changes

The analysis of the shoreline change rate spatial variability in the Tuktoyaktuk Peninsula reveals a consistent overall retreating pattern. Mean change rates varied from −0.50 ± 0.07 m/year to −1.55 ± 0.07 m/year (1950–2020), indicating retreat rates equal to or above the average of −0.50 m/year estimated by Lantuit et al. (2012) for the whole Arctic. The Bols Point, Cutoff Bluff, and Atkinson Point sectors had the highest average retreat rates, with between 42% and 58% of their shoreline retreating more than −1 m/year. The average retreat rates in these sectors, along with Kugmalit Bay, align with those observed on the Yukon Coast, particularly west of Herschel Island, where coasts facing predominant winds also show higher retreat (Irrgang et al. 2018). While wave exposure influences shoreline retreat patterns (Solomon 2005; Lantuit et al. 2012; Whalen et al. 2022), it is not the primary driver of higher retreat in the Tuktoyaktuk Peninsula as most retreat hotspots are located in sheltered areas. Instead, submergence or progressive inundation seems to be driving a higher magnitude of shoreline retreat rates in sheltered areas.

There is great complexity in the spatial patterns of shoreline evolution in the Tuktoyaktuk Peninsula. Some sheltered areas have low retreat rates, such as Kukjuktuk Bay: a large, almost enclosed bay composed of bluffs with low surface degradation; and Seal Bay, Nuvorak Point, and Cape Dalhousie, areas where the breaching of former thermokarst lakes has created a highly sinuous coastline. Sheltered retreat hotspots, such as west Hutchinson Bay, retreated rapidly (–1.3 m/year) despite minimal wave exposure, underscoring submergence's role

In west Hutchinson Bay, a sheltered bay exposed to the east and southwest with high retreat rates, and the lower averages in Warren Point, an area with bluffs and foreshore beaches facing north and northwest. These variations highlight the importance of considering coastal morphology in shoreline evolution studies. The VHR classification of coastal morphology in this study provides greater detail than existing classifications, such as CanCoast (Manson et al. 2019) and the Northern Canada Shoreline Classification (Sergy 2008), which may not provide adequate detail for VHR shoreline change studies.

5.3. Temporal evolution of shoreline change rates

Recent studies across the Arctic have consistently shown an increase in shoreline retreat rates since 2000 (i.e., Farquharson et al. 2018; Irrgang et al. 2018; Jones et al. 2018; Novikova et al. 2018; Cunliffe et al. 2019; Sinitsyn et al. 2020; Gibbs et al. 2021). The Beaufort Sea coast experienced a decrease in retreat rates from the 1970s to the 1990s, followed by an acceleration since the 2000s (Lantuit and Pollard 2008; Radosavljevic et al. 2016; Irrgang et al. 2018; Jones et al. 2018; Gibbs et al. 2021). In the Tuktoyaktuk Peninsula, we observed a 31% increase in average shoreline retreat rates since 1985, affecting 57% of the area, with 57% of the area showing this trend.

Previous shoreline change studies in the Tuktoyaktuk Peninsula have not covered the entire coast. Solomon (2005) studied a coastal section, which includes Kugmalit Bay and part of Toker Point sectors, obtaining a mean shoreline change rate of −0.75 m/year (1972–2000), with a slight increase to −0.84 m/year between 1972 and 1985, followed by a decrease to −0.67 m/year (1985–2000). Our study, covering a broader period, found an overall retreat rate of −1.13 ± 0.07 m/year for the same areas (1950–2020). Specifically, the retreat rates were −0.75 ± 0.15 m/year (1950–1985), consistent with Solomon's earlier findings, increasing to −1.57 ± 0.16 m/year in 1985–2020. This represents a 109% increase in retreat rates for the same areas studied by Solomon, suggesting that most of this increase has likely occurred since 2000.

Several sectors experienced significant increases in retreat rates: Kugmalit Bay (152%), Toker Point (60%), Kukjuktuk Bay (83%), Atkinson Point (84%), and Nuvorak Point (95%). These areas, particularly Kugmalit Bay, Toker Point, and Nuvorak Point, are oriented towards prevailing winds and storms, making them more vulnerable to increased storminess reported in the peninsula (Casas-Prat and Wang 2020; Kim et al. 2021; MacLeod and Dallimore 2021). Arctic warming trends have intensified since the 1980s, leading to increased ground ice melt and permafrost thaw (Irrgang et al. 2022; Rantanen et al. 2022). The high ground ice content in Kugmalit Bay, Toker Point, and Kukjuktuk Bay (Table 8) likely contributed to accelerated retreat rates in these areas since 1985 due to thermokarst processes exacerbated by rapid warming in the Tuktoyaktuk Peninsula (approximately 0.67 °C per decade since 1974), which could result in higher rates of surface degradation through thermokarst processes.

Atkinson Point stands out with an average shoreline change rate of −2.04 ± 0.16 m/year, the highest retreat rates in the Tuktoyaktuk Peninsula and emerging as one of the areas most affected by shoreline retreat in the Beaufort Sea since 1985. This sector displays several areas where retreat trends increased, seven sheltered by offshore barriers or large sandspits and only one exposed. This area, along with others such as Kugmalit Bay, Seal Bay, and Nuvorak Point, shows increased retreat trends primarily in sheltered areas, highlighting the morphological influence of tundra flats driving increased shoreline change trends.

Therefore, this study demonstrates a clear acceleration in shoreline retreat rates along the Tuktoyaktuk Peninsula since 1985, with a 31% increase affecting 57% of the coastline. The trend may have been driven by high ground ice content and rapid warming, which may have enhanced ground ice thaw and thermoerosional processes, particularly in vulnerable sectors such as Kugmalit Bay, Toker Point, and Kukjuktuk Bay. These findings highlight the complexity of Arctic coastal dynamics and the relevance of continued monitoring of its changing drivers under climate change.

Table 11. Average shoreline change rates, land loss area and percentage per coastal morphology class (1950–2020).

	Coastal morphology class	Coverage (%)	EPR (m/year)	Land loss (sq km)	Land loss (%)
Backshore	Tundra flats	29	− 1.09	22	38
	Bluffs with high surface degradation	15	− 0.87	9	17
	Bluffs with low surface degradation	41	− 0.6	17	31
	Barrier beaches and sandspits	15	− 0.77	8	14
Foreshore	Tundra flats	31	− 1.01	22	38
	Beaches	53	− 0.74	28	49
	Active bluffs	16	− 0.62	7	13

Note: EPR, end point rate

Arctic Science Downloaded from cdnsciencepub.com by ENR-ITILIBBF on 10/30/26

5.4. Morphology influence on shoreline evolution—submergence versus erosion

The relationship between coastal morphology and shoreline change rates in the Tuktoyaktuk Peninsula reveals distinct patterns of land loss, with tundra flats, bluffs, and beaches each exhibiting unique rates and contributions to shoreline evolution since 1950 (Table 11). While coastal erosion is widely studied in the Arctic (Couture et al. 2018; Farquharson et al. 2018; Jones et al. 2020; Baranskaya et al. 2021; Terhaar et al. 2021; Irrgang et al. 2022), coastal submergence and its drivers are quite understudied. Submergence refers to the permanent loss of land resulting from vertical processes, such as relative sea-level rise, thaw subsidence, and inundation. This contrasts with erosion, which is driven by lateral sediment removal from wave or current action. Recognising this distinction is essential, as submergence disproportionately impacts low-lying tundra flats or inundated tundra (as observed in similar studies), which has led to higher land loss rates in the Tuktoyaktuk Peninsula.

5.4.1. Bluffs

Our results show that bluff height may enhance shoreline retreat, aligning with reports from the Alaskan Beaufort Sea coast (Gibbs and Richmond 2017; Irrgang et al. 2022). Very low bluffs retreated more rapidly (−0.81 ± 0.07 m/year) than bluffs taller than 2 m (low and medium, −0.50 ± 0.07 m/year and −0.52 ± 0.07 m/year). This likely reflects the fact that lower bluffs are more easily eroded by waves and have less sediment available to buffer future storm impacts (Obu et al. 2016). However, higher bluffs in the southwest, with more ground ice (O'Neill et al. 2022) have experienced accelerated retreat since 1985, likely driven by increased permafrost thaw due to rising air temperatures in the peninsula.

This study also distinguishes bluffs with high surface degradation (−0.87 ± 0.07 m/year) from those with low surficial degradation (−0.60 ± 0.07 m/year) (Table 11), aiming to evaluate the influence of these and their density on bluff retreat. The study suggests that bluffs with high surface degradation in the Tuktoyaktuk Peninsula experienced 45% higher retreat rates compared to bluffs with low surface degradation. This retreat increase can be attributed to the higher susceptibility of bluffs with high surface degradation to block failure and collapse if abraded by the sea in extreme weather events (Barnhart et al. 2014*a*; Hoque and Pollard 2016). However, it is important to note that other factors could also contribute to increased retreat rates. In the foreshore morphology, active bluffs, with a retreat rate of −0.62 ± 0.07 m/year from 1950 to 2020, are more stable than those in the Yukon Coast, which retreated at a rate of −0.8 m/year from 1950 to 2011 (Irrgang et al. 2018).

5.4.2. Tundra flats

Tundra flats backshore represent 29% of the Tuktoyaktuk Peninsula backshore, nearly double the 16% reported for the Yukon coast by Irrgang et al. (2018). These landforms exhibit the highest average shoreline retreat rates in the region, with intertidal inundated flats and wetlands retreating at −1.46 ± 0.07 m/year and inundated tundra flats and polygons at −0.98 ± 0.07 m/year. These rates exceed those reported for the Yukon, with −0.5 m/year for tundra flats and −0.8 m/year for inundated tundra (Irrgang et al. 2018). In extreme cases, shoreline retreat rates reached up to –26 ± 0.07 m/year, comparable to the −25.1 m/year observed in the Alaskan Beaufort Sea Coast (1980s–2010s) (Gibbs and Richmond 2017).

Despite covering 28% of the coast, tundra flats accounted for 38% of total land loss in the 1950–2020 period. This disproportionate loss highlights the dominant role of submergence. Evidence from various low and high tides, such as features visible underwater at high tide, wetlands overtopped, partially submerged polygons, and wetlands and flats lying below the MHWL threshold, consistently points to submergence as the main driver. Progressive inundation and storm surge events, RSL rise (+2.5 mm/year; James et al. 2021James et al. 2021), rising air temperatures, permafrost degradation and thaw subsidence, tectonic and GIA subsidence all contribute to increased retreat rates in tundra flats, especially in intertidal zones, where minimal slope offers little resistance to flooding and storm surges (Olthof et al. 2015; Atkinson et al. 2016; Ford et al. 2016; Greenan et al. 2019; Irrgang et al. 2019, 2022; Lim et al. 2020). Where permafrost and ground ice are present, frequent flooding accelerates per-

Arctic Science Downloaded from cdnsciencepub.com by ENR-ITILIBBF on 10/30/26

mafrost thaw and ground-ice melt, lowering and steepening the nearshore profile (Dallimore et al. 1996; Irrgang et al. 2022). On the Tuktoyaktuk coast, ground subsidence from permafrost thaw has led to volumetric land loss rates up to three times higher than those from coastal erosion alone (Lim et al. 2020; Irrgang et al. 2022).

The Arctic has a microtidal regime, but extreme storm surges and rising sea levels have increased the frequency and extent of flooding, intensifying submergence and thaw processes (Héquette et al. 2001; Hinkel et al. 2014; Irrgang et al. 2022; Whalen et al. 2022). Rising sea levels also elevate the baseline for storm surge flooding and increase the height of extreme wave events, expanding both the area and frequency of these hazards (Hinkel et al. 2014; Lamoreux et al. 2015; Mercer Clarke et al. 2016; Whalen et al. 2022). When combined with active layer deepening, permafrost degradation, and tectonic subsidence, these factors point to a growing trend of submergence-driven land loss throughout the 21st century (Jones et al. 2020; Lim et al. 2020; Irrgang et al. 2022; Nielsen et al. 2022).

Inundated foreshore tundra areas mainly front tundra flats but can also front tundra bluffs or slopes. These areas showed a rate that doubled the Arctic average retreat rate presented by Lantuit et al. (2012). Their irregular and low-lying foreshore zone causes accuracy issues in applying automatic shoreline delineation algorithms, a methodology driving current and upcoming coastal studies (Vos et al. 2023). This raises the importance of human validation of automatic methods or developing methods that distinguish between erosion and submergence.

The distinction between erosion and submergence may be crucial for future studies, as tundra flats prone to submergence exhibit the highest shoreline retreat rates in the Tuktoyaktuk Peninsula: −1.09 m/year (1950–2020) and −1.24 m/year (1985–2020), contributing disproportionately to total land loss while not mobilising sediment (Table 11). Research has extensively addressed carbon fluxes from eroding bluffs and mobilised sediment, but knowledge gaps persist regarding carbon emissions from partially or progressively inundated areas, which may also be significant sources of greenhouse gases due to subsea permafrost thaw and microbial activity (Schuur et al. 2015; Tanski et al. 2019; Irrgang et al. 2022).

5.4.3. Beaches

Foreshore beach change rates registered −0.74 ± 0.07 m/year (Table 11), which is lower than the rate recorded on the Yukon coast (−0.9 m/year) by Irrgang et al. (2018). Foreshore beaches provided some protection to nearby tundra flats by absorbing energy and slowing retreat. In the backshore morphology, barrier beaches and sandspits are the landforms that have registered a higher increase in retreat rates since 1985. However, this increase should be assessed with caution as these landforms have complex morphodynamics, which follow longshore currents (Irrgang et al. 2022). Observations confirm that erosion is the primary process in these areas, with narrowing, berm displacement, and occasional flooding. Unlike tundra flats, however, losses from beaches and barriers directly contribute to sediment remobilisation.

6. Conclusions

This study assesses the shoreline dynamics and its spatiotemporal trends from 1950 to 2020 in the Tuktoyaktuk Peninsula, analysed in three periods: 1950–2020, 1950–1985, and 1985–2020. It also provides a new and updated coastal morphology classification. The backshore is dominated by bluffs with low ice-wedge degradation (41%), followed by tundra flats (28%), Bluffs with high surface degradation (15%) and barrier beaches and sandspits (15%). The foreshore of the Tuktoyaktuk Peninsula is composed of beaches (53%), tundra flats (31%) and active bluffs (16%). Our analysis allowed to draw the following conclusions:

1. Shoreline change rates averaged of −0.77 ± 0.07 m/year, varying between 7.6 ± 0.07 m/year at aggrading sandspits and −26.1 ± 0.07 m/year at inundating low-lying tundra flats. The average retreat rate increased 31%, from −0.67 ± 0.15 m/year in 1950–1985 to −0.88 ± 0.16 m/year in 1985–2020. The Tuktoyaktuk Peninsula lost about 57 square km of land from 1950 to 2020.
2. The retreat rates from 1950 to 2020 were higher in Atkinson Point (−1.55 ± 0.07 m/year), Cutoff Bluff (−1.36 ± 0.07 m/year), and Bols Point (−1.23 ± 0.07 m/year). While these sectors are mostly oriented to the northwest, retreat hotspots in sheltered areas reveal a smaller influence of coastal orientation and wind exposure in shoreline retreat when compared to other areas in the Beaufort Sea Coast.
3. Coastal morphology is a key in shoreline evolution, influencing predominant coastal processes and retreat magnitude. Tundra Flats had the highest retreat rates in both backshore (−1.09 ± 0.07 m/year) and foreshore (−1.01 ± 0.07 m/year), while bluffs with low surface degradation had the lowest backshore retreat rates (−0.60 ± 0.07 m/year). High ice-wedge degradation in bluffs seemingly contributed to increased retreat rates (−0.87 ± 0.07 m/year). Barrier Beaches and Sandspits had a shoreline change rate of −0.77 ± 0.07 m/year. Foreshore beaches with −0.74 ± 0.07 m/year may hinder coastal retreat when fronting tundra flats. Active Bluffs were the most stable foreshore morphology, recording −0.62 ± 0.07 m/year. Very low bluffs retreated at a faster rate (−0.81 ± 0.07 m/year) than bluffs taller than 2 m.
4. The Tuktoyaktuk Peninsula has experienced accelerated shoreline retreat rates since 1985, with an average increase of 31% and 57% of the coast showing negative trends. This includes acceleration in retreat (43.6%), aggradation to retreat (12.7%), and deceleration in aggradation (0.8%). Atkinson Point shows the highest recent retreat rate at −2.04 ± 0.16 m/year (1985–2020). Several sectors, including Kugmalit Bay, Toker Point, Kukjuktuk Bay, Atkinson Point, and Nuvorak Point, have seen retreat rates increase by more than 50% since 1985, influenced by their

low-lying coastal morphology areas, and to a lesser extent, ground ice and coastal exposure.

5. The Tuktoyaktuk Peninsula has a complex and sinuous coastal area where low-lying tundra formations pose no barrier to ocean waters. These areas, located in sheltered areas in the margins of former thermokarst lakes, represent the highest retreat rates and 38% of the land loss from 1950 to 2020, despite representing only 28% of the Tuktoyaktuk Peninsula shoreline. Land loss magnitude has been larger in tundra flats, which are prone to submergence, compared to exposed areas prone to erosion.

This study highlights the importance of existing coastal morphology in controlling shoreline change evolution in the Tuktoyaktuk Peninsula. Data analysis shows that submergence is a key process driving extreme shoreline retreat hotspots, particularly in low-lying areas. The distinction between erosion and submergence is key in Arctic coastal studies, as its differing drivers and impacts must be thoroughly assessed to improve coastal management and climate and morphodynamic models. Future research should focus on integrating sea-level rise, permafrost thaw, and isostatic subsidence alongside erosion in coastal change models. Such an integrated approach would enhance our ability to predict relevant changes affecting local communities and biodiversity. Moreover, it would improve our understanding of how these processes influence sediment, including carbon and contaminant fluxes in Arctic coastal systems, providing valuable insights for climate change assessments and coastal management strategies in rapidly changing Arctic environments.

Acknowledgements

We thank and acknowledge the community of Tuktoyaktuk, including the Hamlet Council, Tuktoyaktuk HTC, and the TC-CRP, for their support and for allowing us to conduct research on their lands. This research was funded under the European Union's Horizon 2020 research and innovation programme under grant agreement no.773421 (project NUNATARYUK), Nuna Project (NE/X005658/1) and by the Centre of Geographical Studies through the Portuguese Foundation for Science and Technology (FCT) under UID/295/2025. Logistical support was provided by Natural Resources Canada and through the Portuguese Polar Program (PROPOLAR) projects TUKCOAST-2024 and TUKCOAST-2025. This research was conducted under the Northwest Territories Scientific permit 16286 and is framed under the College on Polar and Extreme Environments (POLAR2E) of the University of Lisbon. Bernardo Costa was funded by the FCT under the PhD grant 2022.11845.BD. Pléiades imagery was acquired through the ISIS Pléiades Program in connection with the WMO Polar Space Task Group. For the purpose of Open Access, the author has applied a CC-BY public copyright license to any Author's Accepted Manuscript (AAM) version arising from this submission. We thank the anonymous reviewer for the comments that contributed to improving the final version of the manuscript.

Article information

History dates

Received: 25 September 2025
Accepted: 2 June 2026
Accepted manuscript online: 30 June 2026
Version of record online: 18 August 2026

Copyright

© 2026 Author(s) Costa and Vieira; and The Crown. This work is licensed under a Creative Commons Attribution 4.0 International License (CC BY 4.0), which permits unrestricted use, distribution, and reproduction in any medium, provided the original author(s) and source are credited.

Data availability

Data created or analysed in this study namely the Coastal Morphology Classification, the Shorelines and Shoreline Change Rates are available at Zenodo repository (https://doi.org/10.5281/zenodo.20701926).

Author information

Author ORCIDs

Bernardo Costa https://orcid.org/0000-0003-4853-1129
Gonçalo Vieira https://orcid.org/0000-0001-7611-3464
Dustin Whalen https://orcid.org/0000-0002-9965-480X
Michael Lim https://orcid.org/0000-0002-6507-6773

Author contributions

Conceptualization: BC, GV, DW, ML
Data curation: BC, GV, DW, ML
Formal analysis: BC
Funding acquisition: GV, DW, ML
Investigation: BC
Methodology: BC, GV, DW, ML
Project administration: GV, DW, ML
Resources: GV, DW
Supervision: GV, DW, ML
Validation: BC
Visualization: BC
Writing – original draft: BC
Writing – review & editing: BC, GV, DW, ML

Competing interests

The authors declare no competing interests.

Supplementary material

Supplementary data are available with the article at https://doi.org/10.1139/as-2025-0071.

References

Almar, R., Bergsma, E., Maisongrande, P., and de Almeida, L. 2019. Wave-derived coastal bathymetry from satellite video imagery: a showcase with Pleiades persistent mode. Remote Sensing of Environment, **231**: 111263. doi:10.1016/j.rse.2019.111263.

Atkinson, D., Forbes, D., and James, T. 2016. Dynamic coasts in a changing climate. *In* Canada's marine coasts in a changing climate. *Edited by* D.

Arctic Science Downloaded from cdnsciencepub.com by ENR-ITILIBBF on 10/30/26

Arctic Science Downloaded from cdnsciencepub.com by ENR-ITILIBBF on 10/30/26

Lemmen, F. Warren, T. James and C. Mercer-Clarke. Government of Canada, Ottawa, ON. pp.27–68

Baranskaya, A., Novikova, A., Shabanova, N., Belova, N., Maznev, S., Ogorodov, S., and Jones, B.M. 2021. The role of thermal denudation in erosion of ice-rich permafrost coasts in an enclosed bay (Gulf of Kruzenstern, Western Yamal, Russia). Frontiers in Earth Science (Lausanne), **8**: 1–19. doi:10.3389/feart.2020.566227.

Barnhart, K., Anderson, R.S., Overeem, I., Wobus, C., Clow, G.D., and Urban, F.E. 2014a. Modeling erosion of ice-rich permafrost bluffs along the Alaskan Beaufort Sea coast. Journal of Geophysical Research: Earth Surface, **119**: 1155–1179. doi:10.1002/2013JF002845.

Barnhart, K., Overeem, I., and Anderson, R. 2014b. The effect of changing sea ice on the physical vulnerability of Arctic coasts. The Cryosphere, **8**: 1777–1799. doi:10.5194/tc-8-1777-2014.

Barnhart, K., Miller, C., Overeem, I., and Kay, J. 2016. Mapping the future expansion of Arctic open water. Nature Climate Change, **6**: 280–285. doi:10.1038/nclimate2848.

Bartsch, A., Ley, S., Nitze, I., Pointner, G., and Vieira, G. 2020. Feasibility study for the application of synthetic aperture radar for coastal erosion rate quantification across the Arctic. Frontiers in Environmental Science, **8**: 143. doi:10.3389/fenvs.2020.00143.

Berry, H., Whalen, D., and Lim, M. 2021. Long-term ice-rich permafrost coast sensitivity to air temperatures and storm influence: lessons from Pullen Island, Northwest Territories, Canada. Arctic Science, **7**: 723–745, doi:10.1139/as-2020-0003.

Boak, E., and Turner, I. 2005. Shoreline definition and detection: a review. Journal of Coastal Research, **214**: 688–703. doi:10.2112/03-0071.1.

Brady, M.B., and Leichenko, R. 2020. The impacts of coastal erosion on Alaska's North Slope communities: a co-production assessment of land use damages and risks. Polar Geography, **43**: 259–279. doi:10.1080/1088937X.2020.1755907.

Burningham, H., and Fernandez-Nunez, M. 2020. Shoreline change analysis. *In* Sandy beach morphodynamics. *Edited by* D.W.T. Jackson and A.D. Short. Elsevier. pp. 439–460. doi:10.1016/B978-0-08-102927-5.00019-9.

Burvingt, O., Castelle, B., Marieu, V., Lubac, B., Nicolae Lerma, A., and Robin, N. 2025. Using Pleiades satellite imagery to monitor multi-annual coastal dune morphological changes. Remote Sensing (Basel), **17**. doi:10.3390/rs17091522.

Buzard, R.M., Kinsman, N.E., Maio, C.V., Erikson, L.H., Jones, B.M., Anderson, S., et al. 2023. Barrier Island reconfiguration leads to rapid erosion and relocation of a rural Alaska community. Journal of Coastal Research, **39**. doi:10.2112/JCOASTRES-D-22-00093.1.

Casas-Prat, M., Cicon, L., Pouliot, B., Bernier, N.B., Cannon, A.J., and Chan, R. 2024. CanESM5-derived ocean wave projections—considerations for coarse resolution climate models. Ocean Modelling (Oxf), **192**. doi:10.1016/j.ocemod.2024.102430.

Casas-Prat, M., and Wang, X.L. 2020. Projections of extreme ocean waves in the Arctic and potential implications for coastal inundation and erosion. Journal of Geophysical Research: Oceans, **125**. doi:10.1029/2019JC015745.

Clark, A., Moorman, B., Whalen, D., and Fraser, P. 2021. Arctic coastal erosion: UAV-SfM data collection strategies for planimetric and volumetric measurements. Arctic Science, **29**. doi:10.1139/as-2020-0021.

Couture, N., Forbes, D., Fraser, P., Frobel, D., Jenner, K., Manson, G., et al. 2015. A coastal information system for the southeastern Beaufort Sea, Yukon and Northwest Territories. Geological Survey of Canada Open File 7778. doi:10.4095/295975.

Couture, N., Irrgang, A., Pollard, W., Lantuit, H., and Fritz, M. 2018. Coastal erosion of permafrost soils along the Yukon Coastal Plain and fluxes of organic carbon to the Canadian Beaufort Sea. Journal of Geophysical Research: Biogeosciences, **123**: 406–422. doi:10.1002/2017JG004166.

Creel, R., Guimond, J., Jones, B.M., Nielsen, D.M., Bristol, E., Tweedie, C.E., and Paul Overduin, P. 2024. Permafrost thaw subsidence, sea-level rise, and erosion are transforming Alaska's Arctic coastal zone. doi:10.1073/pnas.

Cunliffe, A.M., Tanski, G., Radosavljevic, B., Palmer, W.F., Sachs, T., Lantuit, H., et al. 2019. Rapid retreat of permafrost coastline observed with aerial drone photogrammetry. The Cryosphere, **13**: 1513–1528. doi:10.5194/tc-13-1513-2019.

Dallimore, S., Wolfe, S., and Solomon, S. 1996. Influence of ground ice and permafrost on coastal evolution, Richards Island, Beaufort Sea coast, N.W.T. Canadian Journal of Earth Sciences, **33**: 664–675. doi:10.1139/e96-050.

Diatta, L.S., Schörle, K., Akacha, Z., Bettaieb, S., Drine, A., Oueslati, A., and Lapierre, L. 2025. Performance of segmentation (watershed and meanshift) and image transformation (MNF-laplacian filter) methods for extracting complex coastlines from Pleiades images: the case of the Kerkena archipelago, Tunisia. Frontiers in Remote Sensing, **6**. doi:10.3389/frsen.2025.1542241.

Doherty, Y., Harley, M.D., Vos, K., and Splinter, K.D. 2022. A Python toolkit to monitor sandy shoreline change using high-resolution PlanetScope cubesats. Environmental Modelling & Software, **157**:105512. doi:10.1016/j.envsoft.2022.105512.

Farquharson, L., Mann, D., Swanson, D., Jones, B., Buzard, R., and Jordan, J. 2018. Temporal and spatial variability in coastline response to declining sea-ice in northwest Alaska. Marine Geology, **404**: 71–83. doi:10.1016/j.margeo.2018.07.007.

Forbes, D., Manson, G., Whalen, D., Couture, N., and Hill, P. 2014. Coastal products of marine transgression in cold-temperate and high-latitude coastal-plain settings: Gulf of St Lawrence and Beaufort Sea. Geological Society, London, Special Publications, **388**: 131–163. doi:10.1144/SP388.18.

Ford, J., Bell, T., and Couture, N. 2016. Perspective on Canada's North Coast region. *In* Canada's marine coasts in a changing climate[online]. *Edited by* D. Lemmen, F. Warren, T. James and C. Mercer-Clarke. Government of Canada, Ottawa, ON. pp. 153–206. Available from https://www.mdpi.com/2072-4292/11/19/2212 [accessed March 2025].

Ford, J., Couture, N., Bell, T., and Clark, D. 2018. Climate change and Canada's north coast: research trends, progress, and future directions. Environmental Reviews, **26**: 82–92. doi:10.1139/er-2017-0027.

Gabriel-Robez, C., Lees, R., and Bernard, M. 2012. Pléiades: responsiveness, flexibility, reactivity. International Archives of the Photogrammetry, Remote Sensing and Spatial Information Sciences.

Galley, R.J., Babb, D., Ogi, M., Else, B.G.T., Geilfus, N.-X., Crabeck, O., et al. 2016. Replacement of multiyear sea ice and changes in the open water season duration in the Beaufort Sea since 2004. Journal of Geophysical Research: Oceans, **121**: 1806–1823. doi:10.1002/2015JC011583.

Gibbs, A., Erikson, L., Jones, B., Richmond, B., and Engelstad, A. 2021. Seven decades of coastal change at Barter Island, Alaska: exploring the importance of waves and temperature on erosion of coastal permafrost bluffs. Remote Sensing, **13**: 4420. doi:10.3390/rs13214420.

Gibbs, A., and Richmond, B.M. 2017. National assessment of shoreline change—summary statistics for updated vector shorelines and associated shoreline change data for the north coast of Alaska. U.S. Geological Survey Open-File Report 2017–1107: 1–21. doi:10.3133/ofr20171107.

Greenan, B., James, T., Loder, J., Pepin, P., Azetusu-Scott, K., Ianson, D., et al. 2019. Changes in oceans surrounding Canada. *In* Canada's changing climate report. *Edited by* E. Bush and D. Lemmen. Government of Canada, Ottawa, Ontario. pp.343–423.

Günther, F., Overduin, P.P., Sandakov, A.V., Grosse, G., and Grigoriev, M.N. 2013. Short- and long-term thermo-erosion of ice-rich permafrost coasts in the Laptev Sea region. Biogeosciences, **10**: 4297–4318. doi:10.5194/bg-10-4297-2013.

Günther, F., Overduin, P.P., Yakshina, I.A., Opel, T., Baranskaya, A.V., and Grigoriev, M.N. 2015. Observing Muostakh disappear: permafrost thaw subsidence and erosion of a ground-ice-rich island in response to arctic summer warming and sea ice reduction. Cryosphere, **9**: 151–178. doi:10.5194/tc-9-151-2015.

Hapke, C.J., and Reid, D. 2007. National Assessment of Shoreline Change, Part 4 : historical Coastal Cliff retreat along the California Coast. Pacific Science, 57.

Héquette, A., Desrosiers, M., Hill, P.R., and Forbes, D. 2001. The influence of coastal morphology on shoreface sediment transport under storm-combined flows, Canadian Beaufort Sea. Journal of Coastal Research, **17**: 507–516.

Himmelstoss, E., Henderson, R., Kratzmann, M., and Farris, A. 2018. Digital Shoreline Analysis System (DSAS) version 5.0 user guide. Open-File Report 2018–1179. doi:10.3133/ofr20181179.

Hinkel, J., Lincke, D., Vafeidis, A., Perrette, M., Nicholls, R., Tol, R., et al. 2014. Coastal flood damage and adaptation costs under 21st century sea-level rise. Proceedings of the National Academy of Sciences, **111**: 3292–3297. doi:10.1073/pnas.1222469111.

Arctic Science Downloaded from cdnsciencepub.com by ENR-ITILIBBF on 10/30/26

Hoque, A., and Pollard, W. 2009. Arctic coastal retreat through block failure. Canadian Geotechnical Journal, **46**: 1103–1115. doi:10.1139/T09-058.

Hoque, M.A., and Pollard, W.H. 2016. Stability of permafrost dominated coastal cliffs in the Arctic. Polar Science, **10**: 79–88. doi:10.1016/j.polar.2015.10.004.

Houser, C., Hapke, C., and Hamilton, S. 2008. Controls on coastal dune morphology, shoreline erosion and barrier island response to extreme storms. Geomorphology, **100**: 223–240. doi:10.1016/j.geomorph.2007.12.007.

Irrgang, A., Bendixen, M., Farquharson, L., Baranskaya, A., Erikson, L., Gibbs, A., et al. 2022. Drivers, dynamics and impacts of changing Arctic coasts. Nature Reviews Earth & Environment, **3**: 39–54, doi:10.1038/s43017-021-00232-1.

Irrgang, A., Lantuit, H., Gordon, R., Piskor, A., and Manson, G. 2019. Impacts of past and future coastal changes on the yukon coast—threats for cultural sites, infrastructure, and travel routes. Arctic Science, **5**: 107–126. doi:10.1139/as-2017-0041.

Irrgang, A., Lantuit, H., Manson, G., Günther, F., Grosse, G., and Overduin, P. 2018. Variability in rates of coastal change along the Yukon Coast, 1951 to 2015. Journal of Geophysical Research: Earth Surface, **123**: 779–800. doi:10.1002/2017JF004326.

Itzkin, M., Moore, L.J., Ruggiero, P., Hacker, S.D., and Biel, R.G. 2021. The relative influence of dune aspect ratio and beach width on dune erosion as a function of storm duration and surge level. Earth Surface Dynamics, **9**: 1223–1237. doi:10.5194/esurf-9-1223-2021.

James, T.S., Robin, C., Henton, J.A., and Craymer, M. 2021. Relative sea-level projections for Canada based on the IPCC Fifth Assessment Report and the NAD83v70VG national crustal velocity model. doi:10.4095/327878.

Jones, B., Arp, C., Jorgenson, M., Hinkel, K., Schmutz, J., and Flint, P. 2009. Increase in the rate and uniformity of coastline erosion in Arctic Alaska. Geophysical Research Letters, **36**: 1–5. doi:10.1029/2008GL036205.

Jones, B., Farquharson, L., Baughman, C., Buzard, R., Arp, C., Grosse, G., et al. 2018. A decade of remotely sensed observations highlight complex processes linked to coastal permafrost bluff erosion in the Arctic. Environmental Research Letters, 115001, **13**. doi:10.1088/1748-9326/aae471.

Jones, B., Irrgang, A., Farquharson, L., Lantuit, H., Whalen, D., Ogorodov, S., et al. 2020. Coastal permafrost erosion. NOAA Arctic Report Card, **2020**: 1–10. doi:10.25923/e47w-dw52.

Kim, J., Murphy, E., Nistor, I., Ferguson, S., and Provan, M. 2021. Numerical analysis of storm surges on Canada's western Arctic coastline. Journal of Marine Science and Engineering, **9**: 326. doi:10.3390/jmse9030326.

Lamoreux, S., Forbes, D., Bell, T., Manson, G., Rudy, A., Lalonde, J., et al. 2015. The impact of climate change on infrastructure in the western and central Canadian Arctic. *In* From science to policy in the western and central canadian arctic: an integrated regional impact study (IRIS) of climate change and modernization. *Edited by* G. Stern and A. Gadden. Québec, Quebec.

Lantuit, H., Overduin, P., Couture, N., Wetterich, S., Aré, F., Atkinson, D., et al. 2012. The Arctic coastal dynamics database: a new classification scheme and statistics on Arctic Permafrost coastlines. Estuaries and Coasts, **35**: 383–400. doi:10.1007/s12237-010-9362-6.

Lantuit, H., and Pollard, W. 2008. Fifty years of coastal erosion and retrogressive thaw slump activity on Herschel Island, southern Beaufort Sea, Yukon Territory, Canada. Geomorphology, **95**: 84–102. doi:10.1016/j.geomorph.2006.07.040.

Liew, M., Xiao, M., Jones, B.M., Farquharson, L.M., and Romanovsky, V.E. 2020. Prevention and control measures for coastal erosion in northern high-latitude communities: a systematic review based on Alaskan case studies. Environmental Research Letters, **15**: 093002. doi:10.1088/1748-9326/ab9387.

Lim, M., Whalen, D., Martin, J., Mann, P., Hayes, S., Fraser, P., et al. 2020. Massive ice control on permafrost coast erosion and sensitivity. Geophysical Research Letters, **47**. doi:10.1029/2020GL087917.

MacLeod, R.F., and Dallimore, S.R. 2021. Assessment of storm surge history as recorded by Driftwood in the Mackenzie Delta and Tuktoyaktuk Coastlands, Arctic Canada. Frontiers of the Earth Science (Lausanne), **9**: 1–16. doi:10.3389/feart.2021.698660.

Manson, G., Couture, N., and James, T. 2019. CanCoast 2.0: data and indices to describe the sensitivity of Canada's marine coasts to changing climate. doi:10.4095/314669.

Manson, G., and Solomon, S. 2007. Past and future forcing of Beaufort Sea coastal change. Atmosphere-Ocean ,**45**: 107–122. doi:10.3137/ao.450204.

Mercer Clarke, C., Manuel, P., and Warren, F. 2016. The Coastal Challenge. *In* Canada's marine coasts in a changing climate. *Edited by* D. Lemmen, F. Warren, T. James and C. Mercer Clarke. Government of Canada, Ottawa, ON. pp. 69–98

Meyssignac, B., and Cazenave, A. 2012. Sea level: a review of present-day and recent-past changes and variability. Journal of Geodynamics, **58**: 96–109. doi:10.1016/j.jog.2012.03.005.

Nielsen, D., Pieper, P., Barkhordarian, A., Overduin, P., Ilyina, T., Brovkin, V., et al. 2022. Increase in Arctic coastal erosion and its sensitivity to warming in the twenty-first century. Nature Climate Change, **12**: 263–270, doi:10.1038/s41558-022-01281-0.

Novikova, A., Belova, N., Baranskaya, A., Aleksyutina, D., Maslakov, A., Zelenin, E., et al. 2018. Dynamics of permafrost coasts of Baydaratskaya Bay (Kara Sea) based on multi-temporal remote sensing data. Remote Sensing (Basel), **10**. doi:10.3390/rs10091481.

Obu, J., Lantuit, H., Fritz, M., Pollard, W.H., Sachs, T., and Günther, F. 2016. Relation between planimetric and volumetric measurements of permafrost coast erosion: a case study from Herschel Island, western Canadian Arctic. Polar Research. 30313, **35**. doi:10.3402/polar.v35.30313.

Olthof, I., Fraser, R., and Schmitt, C. 2015. Landsat-based mapping of thermokarst lake dynamics on the Tuktoyaktuk Coastal Plain, Northwest Territories, Canada since 1985. Remote Sensing of Environment, **168**: 194–204. doi:10.1016/j.rse.2015.07.001.

O'Neill, H.B., Wolfe, S.A., and Duchesne, C. 2019. New ground ice maps for Canada using a paleogeographic modelling approach. Cryosphere, **13**: 753–773. doi:10.5194/tc-13-753-2019.

O'Neill, H.B., Wolfe, S.A., and Duchesne, C. 2022. Ground ice map of Canada. doi:10.4095/330294.

O'Rourke, M. 2017. Archaeological site vulnerability modelling: the influence of high impact storm events on models of shoreline erosion in the Western Canadian arctic. Open Archaeology, **3**: 1–16. doi:10.1515/opar-2017-0001.

Pelletier, B., and Medioli, B. 2014. Environmental atlas of the Beaufort coastlands. Geological Survey of Canada, Open File, **7619**: 1–271. doi:10.4095/294601.

Plug, L., Walls, C., and Scott, B. 2008. Tundra lake changes from 1978 to 2001 on the Tuktoyaktuk Peninsula, western Canadian Arctic. Geophysical Research Letters, **35**: 1–5. doi:10.1029/2007GL032303.

Porter, C., Howat, I., Noh, M.-J., Husby, E., Khuvis, S., Danish, E., et al. 2023. ArcticDEM–Mosaics, Version 4.1. Harvard Dataverse. doi:10.7910/DVN/3VDC4W.

Radosavljevic, B., Lantuit, H., Pollard, W., Overduin, P., Couture, N., Sachs, T., et al. 2016. Erosion and flooding—threats to coastal infrastructure in the Arctic: a case study from Herschel Island, Yukon Territory, Canada. Estuaries and Coasts, **39**: 900–915. doi:10.1007/s12237-015-0046-0.

Ramage, J., Jungsberg, L., Meyer, A., and Gartler, S. 2022. 'No longer solid': perceived impacts of permafrost thaw in three Arctic communities. Polar Geography, **45**: 226–239. doi:10.1080/1088937X.2022.2105973.

Rampton, V. 1988. Quaternary Geology of the Tuktoyaktuk Coastlands, Northwest Territories. Geological Survey of Canada, Ottawa, Canada. doi:10.4095/126937.

Rantanen, M., Karpechko, A.Y., Lipponen, A., Nordling, K., Hyvärinen, O., Ruosteenoja, K., et al. 2022. The Arctic has warmed nearly four times faster than the globe since 1979. Communications Earth & Environment 2022 3:1 **3**: 1–10. doi:10.1038/s43247-022-00498-3.

Schuur, E.A.G., McGuire, A.D., Schädel, C., Grosse, G., Harden, J.W., Hayes, D.J., et al. 2015. Climate change and the permafrost carbon feedback. Nature, **520**: 171–179. doi:10.1038/nature14338.

Sergy, G. 2008. The shoreline classification Scheme for SCAT and oil spill response in Canada. Proceedings of the 31stArctic and Marine Oil Spill Program Technical Seminar. Ottawa, Ontario, Canada.

Sinitsyn, A., Guegan, E., Shabanova, N., Kokin, O., and Ogorodov, S. 2020. Fifty four years of coastal erosion and hydrometeorological parameters in the Varandey region, Barents Sea. Coastal Engineering, **157**: 103610. doi:10.1016/j.coastaleng.2019.103610.

Smith, K.E.L., Terrano, J.F., Pitchford, J.L., and Archer, M.J. 2021. Coastal wetland shoreline change monitoring: a comparison of shorelines from high-resolution worldview satellite imagery, aerial imagery, and field surveys. Remote Sensing (Basel), **13**. doi:10.3390/rs13153030.

Solomon, S. 2005. Spatial and temporal variability of shoreline change in the Beaufort-Mackenzie region, northwest territories, Canada. Geo-Marine Letters, **25**: 127–137. doi:10.1007/s00367-004-0194-x.

Tanguy, R., Whalen, D., Prates, G., and Vieira, G. 2023. Shoreline change rates and land to sea sediment and soil organic carbon transfer in eastern Parry Peninsula from 1965 to 2020 (Amundsen Gulf, Canada). Arctic Science, **2020**: 1–20. doi:10.1139/AS-2022-0028.

Tanski, G., Wagner, D., Knoblauch, C., Fritz, M., Sachs, T., and Lantuit, H. 2019. Rapid CO2 release from eroding permafrost in seawater. Geophysical Research Letters, **46**: 11244–11252. doi:10.1029/2019GL084303.

Terhaar, J., Lauerwald, R., Regnier, P., Gruber, N., and Bopp, L. 2021. Around one third of current Arctic Ocean primary production sustained by rivers and coastal erosion. Nature Communications, **12**: 1–10. doi:10.1038/s41467-020-20470-z.

Timmermans, M.-L., and Labe, Z. 2020. Sea surface temperature [in "Arctic Report Card 2020"]. NOAA Arctic Report Card, **2020**: 53–57. doi:10.25923/v0fs-m920.

Trishchenko, A.P., Kostylev, V.E., Luo, Y., Ungureanu, C., Whalen, D., and Li, J. 2022. Landfast ice properties over the Beaufort Sea region in 2000–2019 from MODIS and Canadian Ice Service data. Canadian Journal of Earth Sciences, **59**: 847–865. doi:10.1139/cjes-2021-0011.

Tuck, M., Dickson, M., Ryan, E., Ford, M., and Konlechner, T. 2024. A national scale coastal change dataset for Aotearoa New Zealand. Data in Brief, **57**:111104. doi:10.1016/j.dib.2024.111104.

Vermaire, J.C., Pisaric, M.F.J., Thienpont, J.R., Courtney Mustaphi, C.J., Kokelj, S.V., and Smol, J.P. 2013. Arctic climate warming and sea ice declines lead to increased storm surge activity. Geophysical Research Letters, **40**: 1386–1390. doi:10.1002/grl.50191.

Vitousek, S., Buscombe, D., Vos, K., Barnard, P.L., Ritchie, A.C., and Warrick, J.A. 2023. The future of coastal monitoring through satellite remote sensing. Cambridge Prisms: Coastal Futures, **1**. doi:10.1017/cft.2022.4.

Vos, K., Splinter, K.D., Palomar-Vázquez, J., Pardo-Pascual, J.E., Almonacid-Caballer, J., Cabezas-Rabadán, C., et al. 2023. Benchmarking satellite-derived shoreline mapping algorithms. Communications Earth & Environment, **4**: 345. doi:10.1038/s43247-023-01001-2.

Ward Jones, M.K., Pollard, W.H., and Jones, B.M. 2019. Rapid initialization of retrogressive thaw slumps in the Canadian high Arctic and their response to climate and terrain factors. Environmental Research Letters, **14**. doi:10.1088/1748-9326/ab12fd.

Whalen, D., Forbes, D.L., Kostylev, V., Lim, M., Fraser, P., Nedimovic, M.R., and Stuckey, S. 2022. Mechanisms, volumetric assessment, and prognosis for rapid coastal erosion of Tuktoyaktuk Island, an important natural barrier for the harbour and community. Canadian Journal of Earth Sciences, **59**: 945–960. doi:10.1139/cjes-2021-0101.

Wolfe, S., Murton, J., Bateman, M., and Barlow, J. 2020. Oriented-lake development in the context of late quaternary landscape evolution, McKinley Bay Coastal Plain, western Arctic Canada. Quaternary Science Reviews, **242**: 106414. doi:10.1016/j.quascirev.2020.106414.

Wolfe, S.A., O'Neill, H.B., and Duchesne, C. 2021. A ground ice atlas of Canada. doi:10.4095/328115.

Yang, M., Qiu, Y., Huang, L., Cheng, M., Chen, J., Cheng, B., and Jiang, Z. 2023. Changes in sea surface temperature and sea ice concentration in the Arctic Ocean over the past two decades. Remote Sensing, **15**: 1095. doi:10.3390/rs15041095.

Zagórski, P., Jarosz, K., and Superson, J. 2020. Integrated assessment of shoreline change along the Calypsostranda (Svalbard) from Remote sensing, Field survey and GIS. Marine Geodesy, **43**: 433–471. doi:10.1080/01490419.2020.1715516.

Zwieback, S., Kokelj, S.V., Günther, F., Boike, J., Grosse, G., and Hajnsek, I. 2018. Sub-seasonal thaw slump mass wasting is not consistently energy limited at the landscape scale. The Cryosphere, **12**: 549–564. doi:10.5194/tc-12-549-2018.

Arctic Science Downloaded from cdnsciencepub.com by ENR-ITILIBBF on 10/30/26